P-T-T HISTORY OF THE AMASIA AND STEPANAVAN SUB-OPHIOLITIC METAMORPHIC UNITS (NW ARMENIA, LESSER CAUCASUS): IMPLICATIONS FOR METAMORPHIC SOLE DEVELOPMENT AND FOR THE OBDUCTION PROCESS

Marc Hässig*,°,✉, Yann Rolland°, Raphael Melis°, Marc Sosson°, Ghazar Galoyan** and **Olivier Bruguier*****

* *Department of Earth Sciences, University of Geneva, Switzerland.*
** *Institute of Geological Sciences, National Academy of Sciences of Armenia, Yerevan, Armenia.*
*** *Géosciences Montpellier, UMR 5243-CC 60, Université Montpellier, France.*
° *Université Côte d'Azur, CNRS IRD, Observatoire de la Côte d'Azur, Valbonne, France.*
✉ *Corresponding author, email: Marc.Haessig@unige.ch*

Keywords: *obduction; ophiolite; metamorphic sole; P-T-t path; Northern Neotethys; Lesser Caucasus.*

ABSTRACT

The Sevan-Akera suture zone ophiolites are relics of a vast ophiolitic nappe which testifies a major obduction event, up to 300 km of horizontal transport, of the northern branch of Neotethys oceanic crust over the South Armenian/Taurides continental block. Near the locality of Amasia (NW Armenia), garnet-bearing amphibolites are preserved within a greenschist facies tectonic mélange unit located below the non-metamorphic obducted oceanic unit. The garnet amphibolites show two parageneses: (1) garnet-amphibole-plagioclase granoblasts which crystallized along the S_1 foliation intensely folded and recrystallized into (2) epidote-chlorite-phengite during retrogression and S_2 deformation. S_1 and S_2 deformation stages feature top-to-the-South ductile shearing, interpreted as the motion of the ophiolite nappe during obduction. Thermobarometry reveals a metamorphic history with two P-T fields: (1) an amphibolite stage, T = 600±20°C and 6 ≤ P ≤ 7 kbar, followed by (2) a greenschist stage, T = 350±30°C and 1.25 ≤ P ≤ 4.5 kbar. $^{40}Ar/^{39}Ar$ dating on amphiboles and white micas yields similar within-error ages of 88-92±2 Ma. U-Pb dating on rutile yields an age of 90.2±5.2 Ma. These results are complemented by new and pre-existing characterizations of lithologies in a similar structural position 40 km east, in the locality of Stepanavan. There, newly identified eclogite yield metamorphic conditions of T = 575±25°C and 17.5 ≤ P ≤ 20 kbar. The P-T-t history of these metamorphic units argues for a rapid tectonic process featuring intra-oceanic subduction below a relatively hot oceanic lithosphere, slicing of the overriding oceanic domain, underplating of this subducted material along the hanging wall of the subduction zone and formation of a metamorphic sole as part of an 'obduction channel'.

INTRODUCTION

There is still much controversy concerning the explanation of oceanic lithosphere obduction initiation and subsequent transport onto the continental crust (e.g., Agard et al., 2014; Duretz et al., 2015; Hässig et al., 2016a; 2016b; 2017). Obducted ophiolite sequences generally include thick slices of undeformed oceanic lithosphere originating from a supra-subduction zone setting, detached from its mantle basement and emplaced over a continental margin (Coleman, 1971; Dewey, 1976; Spray, 1983). Models for obduction initiation include an early stage of oceanic lithosphere buckling (Agard et al., 2007) or ridge subduction (Coleman, 1976; Hacker, 1991), leading to intra-oceanic thrusting, which may result in the development of a metamorphic sole (e.g., Hacker, 1990; Michard et al., 1991;Gnos, 1993). Models also feature intra-oceanic subduction which continues to a 'marginal' stage at which point the oceanic lithosphere is thrust over the passive continental margin or under-plated by the latter (Dilek and Whitney, 1997; Gray and Gregory, 2000; Engi et al., 2001; Bortolotti et al., 2005). The relative position of intra-oceanic thrusting initiation, the particular physical and/or geochemical properties of the lithologies composing the involved oceanic lithospheres (e.g., the role of mantle flows and plume events leading to oceanic plateau emplacement; Vaughan and Scarrow, 2003; Hässig et al., 2016a; 2916b) and geodynamic settings recorded throughout the metamorphic processes are still subject to debate (e.g., Agard et al., 2007; 2014; Duretz et al., 2015).

The reconstruction of the geodynamic evolution of oceanic basins that were formed in the Neyethyan domain allows a better understanding of the role of the dominant factors involved in oceanic closure, including obduction processes. Key examples of obducted ophiolite sequences are found throughout the Tethyan collisional belts (*Oman*: Coleman, 1976; Hacker et al., 1996; Searle and Cox, 1999; *Northern Albania*: Carosi et al., 1996; Gaggero et al., 2009; *Turkey-Caucasus-Iran*: Adamia et al., 1981; Barrier and Vrielynck, 2008; *Turkey*: Göncüoğlu and Turhan, 1984; Hempton, 1985; Lytwyn and Casey, 1995; Okay et al., 2001; Oberhänsli et al., 2010; 2014; Parlak et al., 2013; Yılmaz et al., 2014; *Eastern Turkey-Lesser Caucasus*: Rolland et al., 2012; *Lesser Caucasus*: Zakariadze et al., 1990; Galoyan et al., 2007; 2009; *south Central Tibet*: Ding et al., 2005; Guilmette et al., 2009). The most studied example is the Oman ophiolite, which is exceptionally well preserved, and has led to detailed reconstructions of the obduction process (Agard et al., 2014, and references therein). However, the obduction model developed for this 'case example' (e.g., Duretz et al., 2015) needs to be tested with other obduction examples. The history of Central and Northern Neotethyan ophiolites seems quite different to that of the Oman ophiolite. The oceanic lithosphere preserved in the Oman ophiolite was formed within 20 Myr before its obduction, while the lithologies forming the Lesser Causasian and Northeastern Anatolian ophiolites are about 80 Myr older than onset of their obduction (Hässig et al., 2013b; 2016a; 2016b; 2017). The Lesser Caucasus region (Figs. 1 and 2) presents all the key features to decipher the precise proceeding

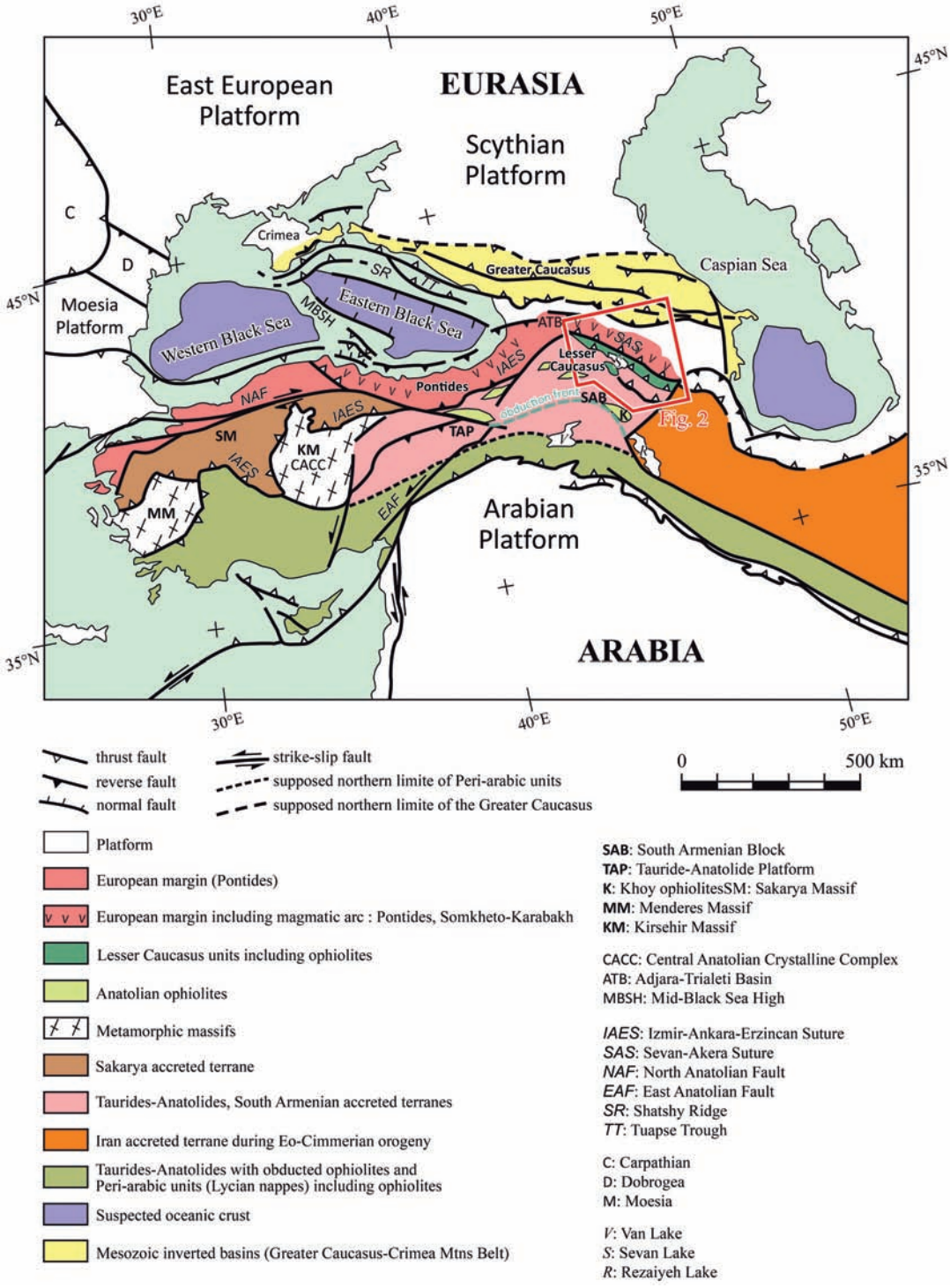

Fig. 1 - Tectonic map of the Middle East - Caucasus area, with main blocks and suture zones, after Hässig et al. (2013a). Location of Fig. 2 is indicated.

of obduction, leading to widespread outcrops of intact ophiolites (e.g., Dercourt et al., 1986) and of metamorphic rocks ('metamorphic sole') found directly underneath the ophiolite nappes, whose formation is ascribed to obduction initiation and ophiolite emplacement (e.g., Hacker, 1990; Dilek and Whitney, 1997; Elitok and Drüppel, 2008). Such 'suture zone' lithologies provide key timing and palaeogeographic data for geodynamic reconstructions of the obduction process. Furthermore, their geometry and geochemistry provide key information to reconstruct the nature of former oceanic domains, needed for tectonic reconstructions (e.g., Ricou et al., 1985; Stampfli et al., 2001; Stampfli and Borel, 2002; Barrier and Vrielynck, 2008; Barrier et al., 2018).

The Lesser Caucasus region (Figs. 1 and 2), particularly the Armenian part, features intact and unmetamorphosed sections of obducted oceanic crust, which formed during mid-Jurassic times only slightly affected by the later collisional history (c. 180 ~ 150 Ma; Galoyan et al., 2009; Rolland et al., 2009b; 2010; Hässig et al., 2013a; 2017). They feature both a metamorphic sole and an intact sedimentary obduction front enabling the reconstruction of part of the obducted ophiolite nappe's geometry, emplacement timing and overall kinematics (Sosson et al., 2010; Rolland et al., 2012; Hässig et al., 2013a).

In this paper, we report new structural, petrologic, geochemical as well as $^{40}Ar/^{39}Ar$ and U-Pb chronological data

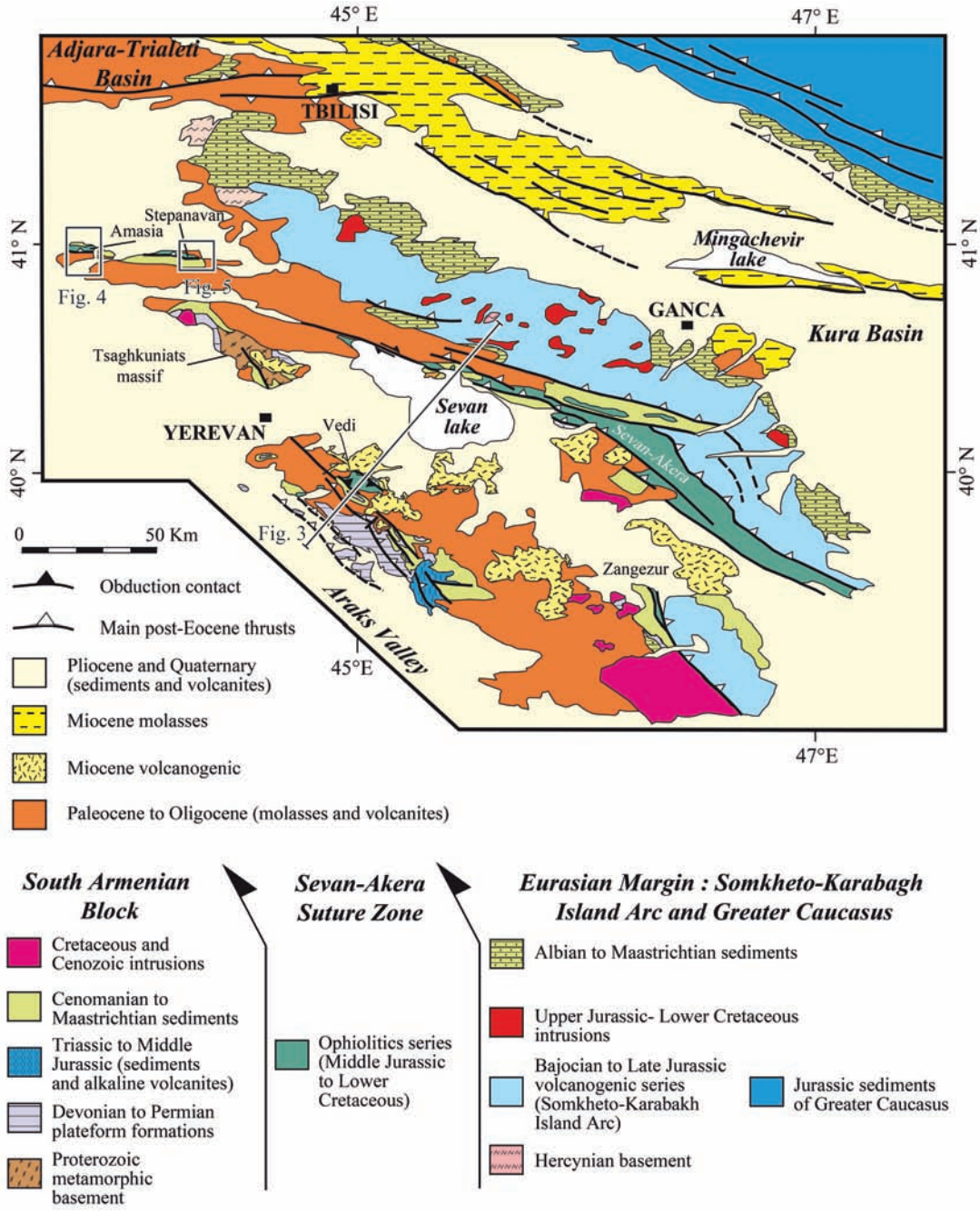

Fig. 2 - Structural map of the Lesser Caucasus modified from Sosson et al. (2010), after Hässig et al. (2013a). Location is indicated on Fig. 1. The position of geological section Fig. 3 and the maps Fig. 4 and 5 are also shown.

obtained from sub-ophiolitic metamorphic units (eclogites and garnet amphibolites). The studied rocks crop out in a tectonic mélange at the base of the tectonic contact of the ophiolites in the localities of Stepanavan and Amasia (approximately 40 km from one another along the Sevan-Akera Suture in NW Armenia; Fig. 2) exhumed by way of a post-obduction collision related thrust (Galoyan et al., 2007; Rolland et al., 2009a; Hässig et al., 2013a; 2013b; 2017). The results of geochemical analyses obtained on these metamorphic rocks provide insights for the nature and geodynamic setting of their protolith. The Pressure-Temperature-time (P-T-t) reconstructions provide insight concerning temperature variations and burial/exhumation rates of these units throughout their metamorphic cycle, which comprises intra-oceanic subduction and subsequent ophiolite emplacement. These data complement previous P-T-t estimates of other metamorphic rocks cropping out in the same structural position in the area of Stepanavan, featured in Rolland et al. (2009a). Based on this new data pertaining to these metamorphic units, we propose a geodynamic reconstruction for the obduction process along this portion of the Northern Neotethyan Suture, and for the emplacement of the Lesser Caucasus ophiolites in Armenia.

GEOLOGICAL SETTING

The Middle East-Caucasus area (Fig. 1) can be divided into three main sectors, from north to south:

(1) The European platform, whose southern margin is characterized by the Pontides and Somkheto-Karabargh magmatic arcs (e.g., Adamia et al., 1981; Rolland et al., 2016; Okay and Topuz, 2017).

(2) Accreted terranes of Gondwanan origin, including the South Armenian Block (SAB; Knipper, 1975; Knipper and Khain, 1980; Hässig et al., 2015a). The SAB likely

represents the eastern continuation of the Taurides-Anatolides Platform (TAP; Sengör and Yılmaz, 1981). The northern and southern limits of this sector are underlined by Northeastern Anatolian-Lesser Caucasus and peri-arabic units, respectively, which both feature ophiolite belts.

(3) The Arabian platform, to the south of the studied area, whose collision with the TAP completely closed the Tethyan realm along this portion of the Alpine-Himalayan Belt.

The Middle East-Caucasus area is characterized by two distinct suture zones, the Northern Tethyan (Izmir-Ankara-Erzincan, IAES, and Amasia-Sevan-Akera, SAS, respectively) and the Southern Tethyan (Misis-Andirin, Bitlis and Zagros) Sutures. They result from the closure of the Paleotethys and northern branch of the Neotethys to the north and the southern branch of the Neotethys to the south of the SAB-TAP, respectively (e.g., Rolland et al., 2012).

Along the Izmir-Ankara-Erzincan-Amasia-Sevan-Akera Suture zone (IAES-SAS), ophiolites represent preserved relics of the fully closed Northern Neotethyan oceanic domain (see a review in Hässig et al., 2017), with a well-preserved subduction channel interplate contact (Hässig et al., 2016c). These ophiolites show a Jurassic-Early Cretaceous age and bear multiple geochemical tendencies, interpreted as reflecting formation in a supra-subduction context (Bortolotti and Sagri, 1968; Palandjyan, 1971; Sokolov, 1977; Zakariadze et al., 1983; Knipper et al., 1986; Galoyan et al., 2007; 2009; Rolland et al., 2009b). Furthermore, subduction-related metamorphic rocks are found along this suture zone, which provide insights for Jurassic (Topuz et al., 2013a; 2013b) and Cretaceous (Rolland et al., 2009a) subductions.

Timing of the obduction

Obduction occurred at 90-83 Ma in all of the East Anatolia-Armenia region (see a synthesis in Hässig et al., 2013b and references therein). Coniacian to Santonian (90-83 Ma) obduction onto the SAB is marked by flysch series reworking the ophiolites at the obduction front and reef series of similar age sealing the obducted nappe in the southern part of the SAB (Vedi area: Sokolov, 1977; Sosson, et al., 2010; Danelian et al., 2014; Figs. 2 and 3). Geological observations imply that at least two north dipping subduction zones were active at the same time north of the SAB: (1) an intra-oceanic zone and (2) farther north another zone along the southern Eurasian margin (Sosson et al., 2010; Rolland et al., 2011; 2016;). After ophiolite emplacement, the Northern Neotethys Ocean was not yet fully closed as indicated by paleomagnetism data. A maximum of 1000 km subsisted between the SAB and the Eurasia margin after the obduction event (Meijers et al., 2015). Thus, obduction preceded a final subduction stage before onset of the collision-accretion of the SAB-TAP to the Southern Eurasian margin during the Late Cretaceous-Paleogene (Rolland et al., 2009b; 2011; Sosson et al., 2010; Mederer et al., 2013; Meijers et al., 2017). Afterwards, the Arabia-TAP/SAB collision occurred during the Late Eocene (Yilmaz et al., 1993; Okay et al., 2001; Rice et al., 2009; Agard et al., 2010; Rolland et al., 2012; Pourteau et al., 2013; Sosson et al., 2016;). Cenozoic volcanism (Moritz et al., 2016; Rezeau et al., 2016; 2017; Sahakyan et al., 2017;) largely masks the ophiolites, but due to the recent onset of hard collision, only limited collisional deformation affected the obducted nappe structure.

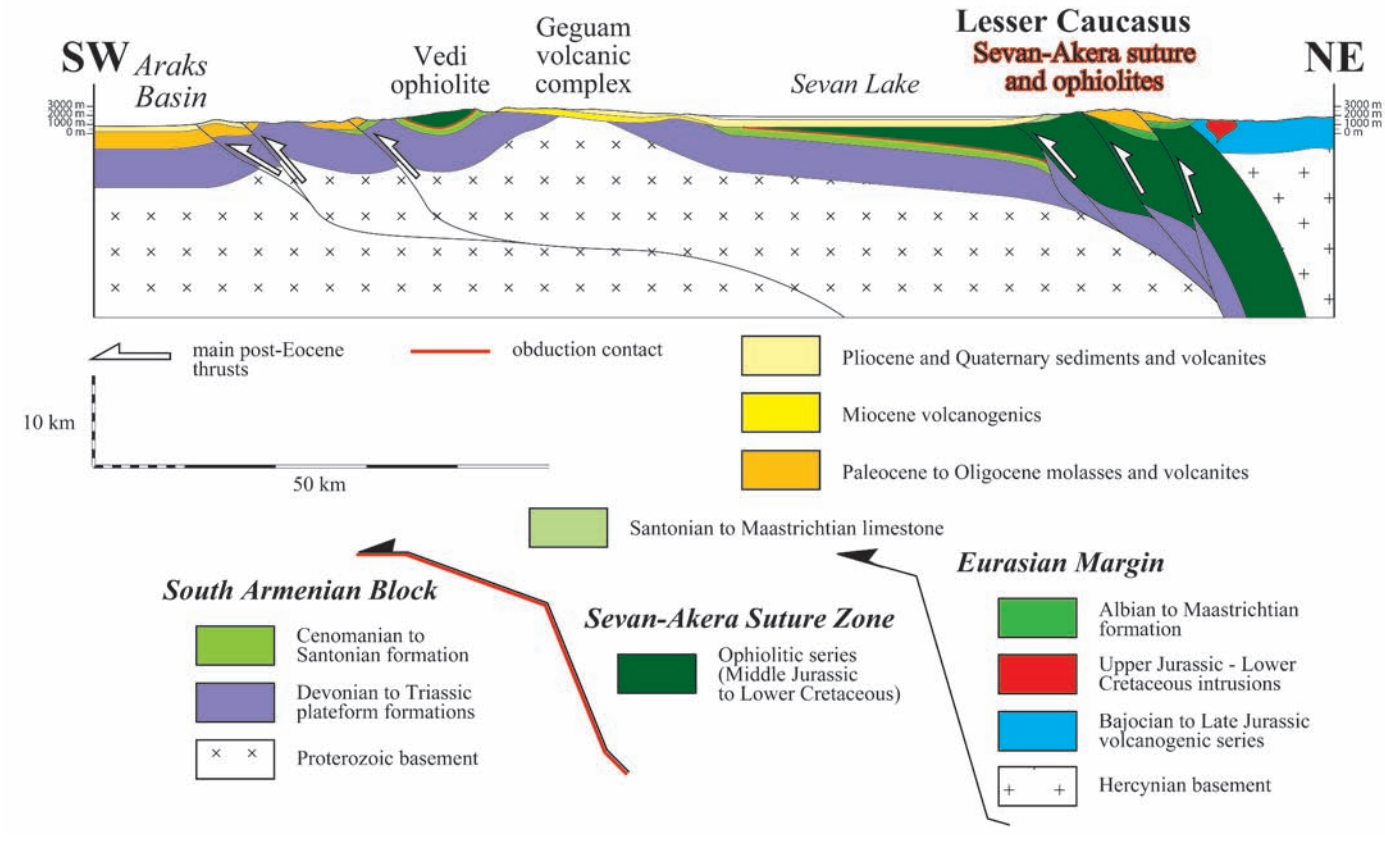

Fig. 3 - Interpretative crustal-scale sketch cross-section of the Armenia-Azerbaijan transect, after Hässig et al. (2013a), modified. Location of the figure is indicated on Fig. 2.

Structure of the ophiolite

For a synthesis concerning the Lesser Caucasus ophiolites, we refer to Galoyan et al. (2007; 2009), Rolland et al. (2009b; 2010), Sosson et al. (2010) and Hässig et al. (2013a, 2013b; 2017), These works document outcrops of gabbro intruding serpentinites dated at c. 175-165 Ma. They are overlaid by basalts with tholeiitic compositions contaminated by subduction components and as well as radiolarites of similar age (Middle-early Late Jurassic; Danelian et al., 2007; 2008; 2010; 2012; Asatryan et al., 2010). Pillow lavas of alkaline Ocean Island Basalt (OIB) emplaced in the Early Cretaceous times in a marine environment can be found directly above these series, prior to their obduction (Rolland et al., 2009b).

Description of the study areas

The study areas lie in the north-eastern Lesser Caucasus, near the villages of Amasia and Stepanavan in Northwestern Armenia (Figs. 2, 4 and 5). There, the Northern Neotethyan ophiolites crop out in tectonic windows through Cenozoic

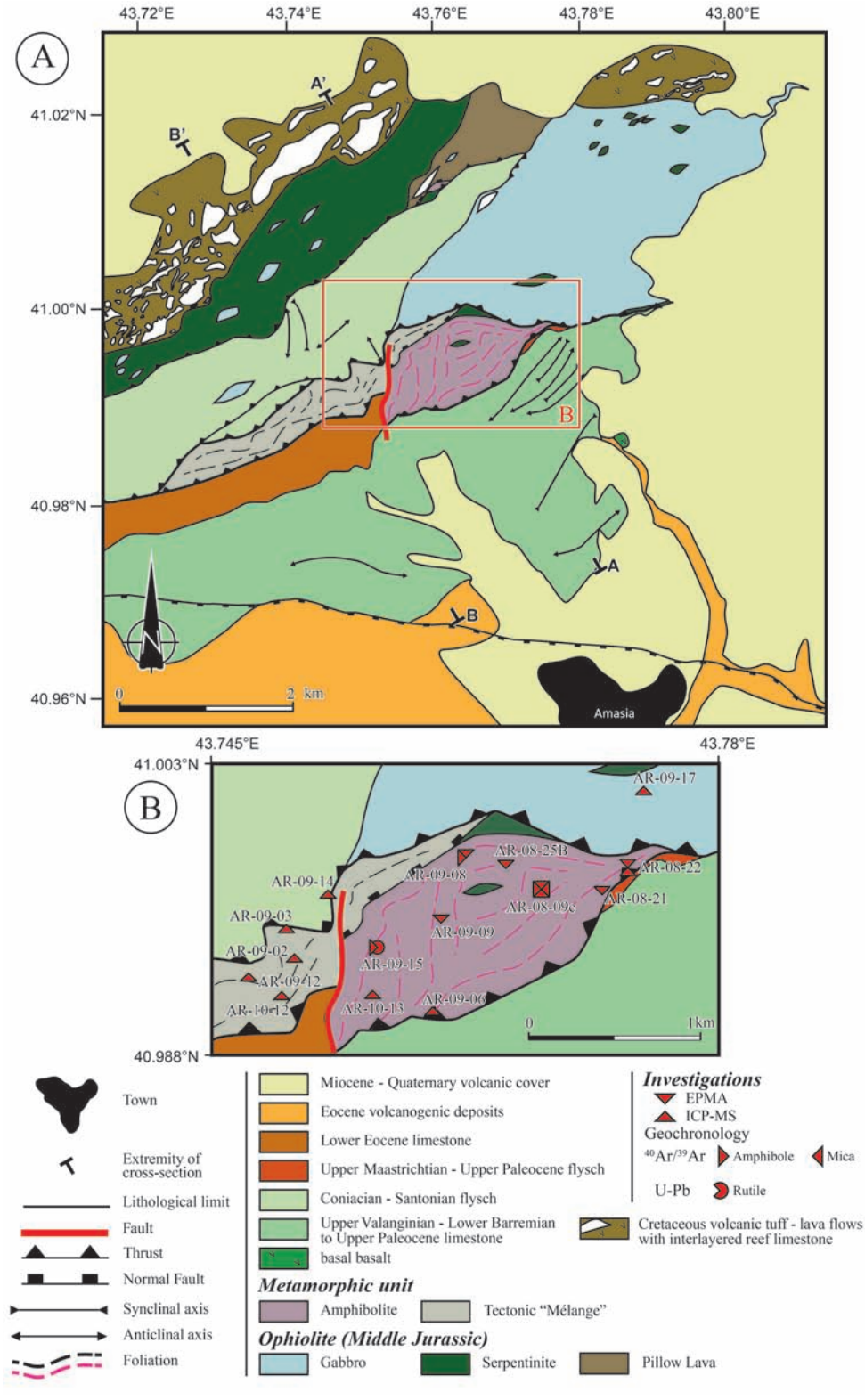

Fig. 4 - Structural maps of the Amasia ophiolite window, after Hässig et al. (2013a), modified. Location of the figure is indicated on Fig. 2. (A), Large map of the Amasia ophiolite; the locations of the geological sections A-A' and B-B' of Figs. 6A and 6B, respectively, are indicated. (B), enlarged map of the sub-ophiolitic metamorphic unit of Amasia (garnet amphibolites); the locations of samples analyzed by EPMA, ICP-MS geochemistry as well as $^{40}Ar/^{39}Ar$ and U-Pb geochronology methods of Figs. 8, 9, 10 and 12 are indicated.

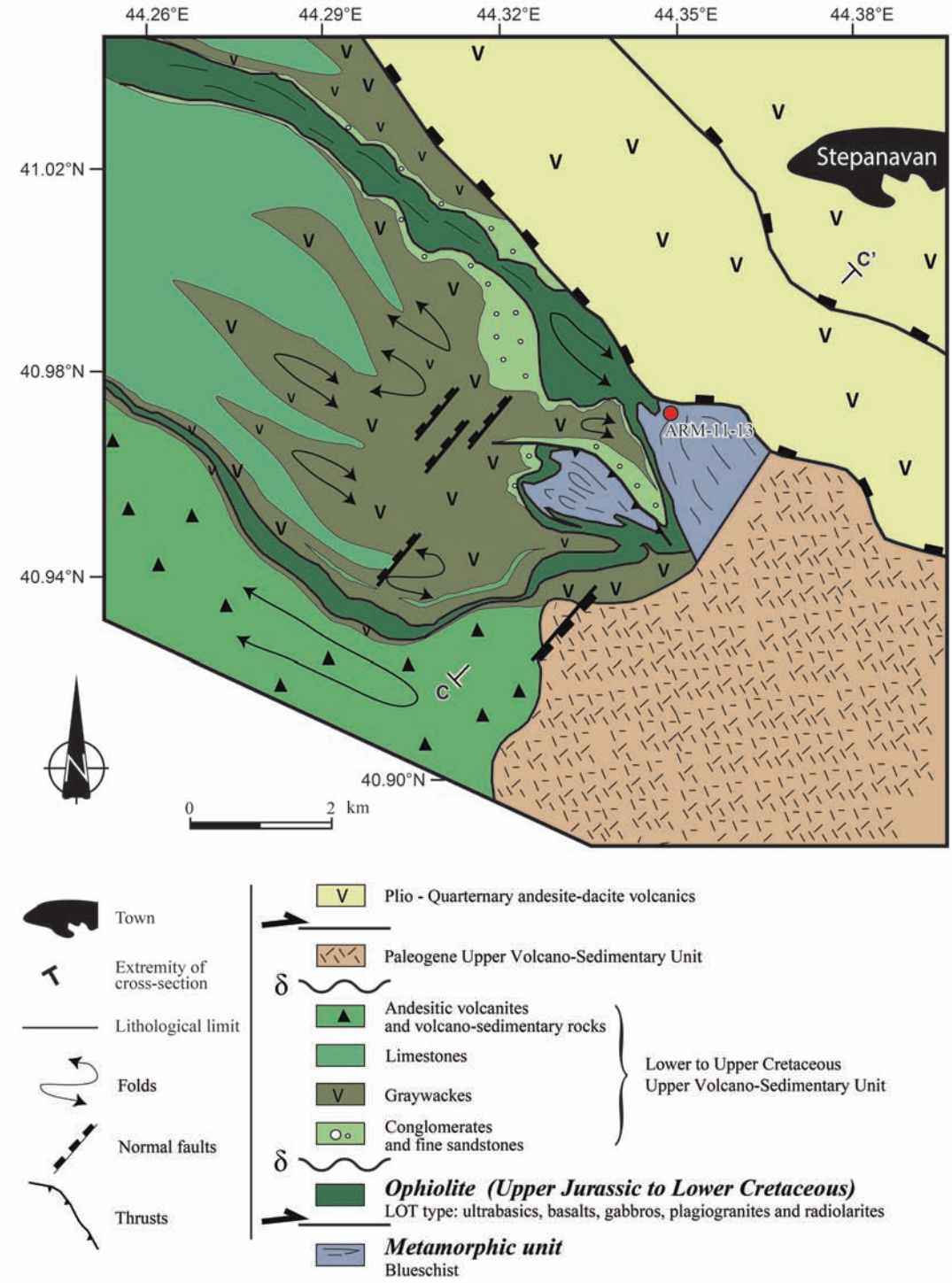

Fig. 5 - Structural maps of the Stepanavan ophiolite window, after Rolland et al. (2009a), modified. Location of this figure is indicated on Fig. 2. The location of the geological cross-section C-C' of Fig. 6C as well as the location sample ARM-11-13 are indicated.

thrusts and normal faults, fully described in Rolland et al. (2009a) and Hässig et al. (2013a). In this paper, we focus on the sub-ophiolitic metamorphic rocks, which likely recorded the variations in P-T conditions prevailing at the base of the obduction.

In Amasia, a tectonic mélange is found underneath this ophiolitic series. The tectonic mélange is made of sheared serpentinites, gabbros, basaltic lavas and metasediments, metamorphosed in the greenschist facies (Hässig et al., 2013a). A unit of garnet-bearing amphibolites occurs tectonically below, or within, this latter unit (Fig. 4). A full description of the structural relations of this unit with the rest of the Amasia ophiolite is provided in Hässig et al. (2013a).

In Stepanavan (Fig. 5), East of Amasia, ophiolites have been described in association with blueschists and amphibolite facies metamorphic rocks (Galoyan etal., 2007; Rolland et al., 2009a). These metamorphic rocks are dated by $^{40}Ar/^{39}Ar$ on phengite (1) at 94-91 Ma, interpreted as the age of high pressure (HP) peak and (2) at 73-71 Ma, interpreted as the age of retrogression in low pressure and medium temperature conditions (LP-MT) ascribed to a lower amphibolite facies (HP: P = 12±1.5 kbar, T = 545±60°C; LP-MT: P = 5.7±0.2 kbar, T = 505±67°C; Rolland et al., 2009a). Unfortunately no age was determined for later retrogression in low pressure and low temperature conditions (LP-LT) in a greenschist facies attested by a distinct mineral assemblage

(Rolland et al., 2009a). In association to these metamorphic rocks, in this study we report eclogite facies rocks. These metamorphic rocks evidence the presence of a subduction zone active during the Middle Cretaceous, which stopped in the Late Cretaceous at 80-75 Ma (Rolland et al. 2011).

According to the field observations, the geological map and cross-sections (Figs. 4, 5 and 6), both areas feature:

1 - An ophiolitic unit constituted by serpentinites, gabbros, basaltic pillow lavas and volcanic rocks with interlayered reef limestones. This unit represents an un-metamorphosed obducted oceanic crust section formed during Middle and Late Jurassic times, dated mid/late Oxfordian to late Kimmeridgian/early Tithonian (163-150 Ma) by age-diagnostic radiolarian identification in Stepanavan (Danelian et al., 2007) and in Amasia (Danelian et al., 2016). Dating of gabbro amphiboles by $^{40}Ar/^{39}Ar$ yielded 169.0±4.6 to 175.8±3.9 Ma in Amasia (Hässig et al., 2013a).

2 - A sub-ophiolitic metamorphic unit composed of meta-basalts, meta-sediments and serpentinites. In Amasia elongated boudins of marbleized limestones along with serpentinites and meta-basalts indicate a top-to-south sense of shear. Amphibolites show a penetrative S_1 foliation marked by amphibole and garnet-rich dark coloured layers alternating with plagioclase and quartz-rich light coloured layers. This alternation defines syn-metamorphic SC shear bands (Fig. 7). An S_2 foliation and lineation is also present, marked by chlorite and phengite as well as amphibole and rolled garnet. These evidence that this unit was tectonized

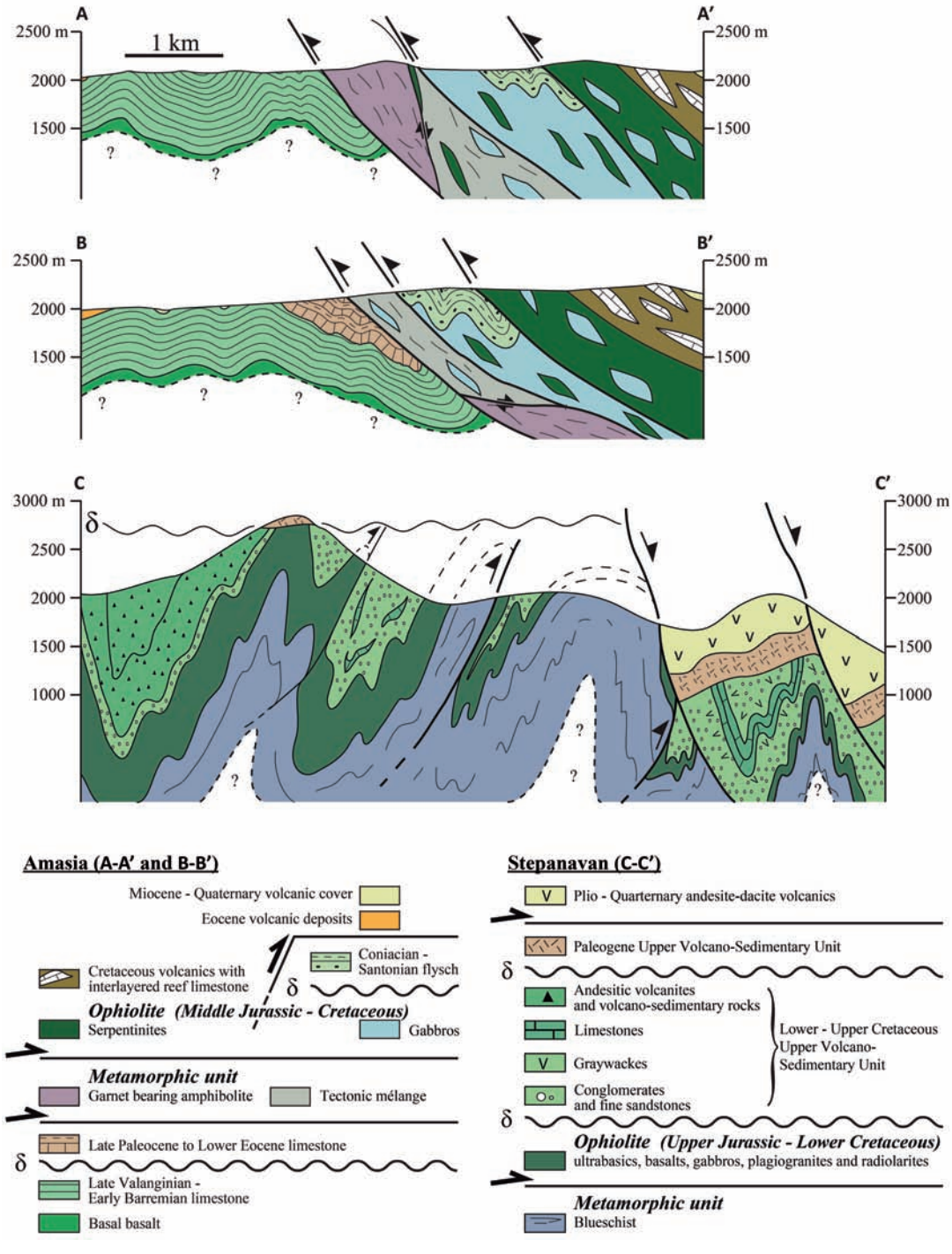

Fig. 6 - Cross-sections illustrating the makeup of main units and the geometry of the Amasia (A-A' and B-B') and Stepanavan (C-C') ophiolites, after Rolland et al. (2009a) and Hässig et al. (2013a), respectively. Locations are indicated on Figs. 4 and 5.

(deformed) during at least two phases. Both phases, responsible for the formation of S_1 and S_2, are coherent with southward sense of shear during thrusting (Fig. 7).

In Stepanavan, blueschists and eclogites are mainly composed of boudins of glaucophane-bearing meta-volcanic rocks and meta-sediments (micaschists, marbles, metaconglomerates, quartzites, and rare gneiss blocks) (Roland et al., 2009a).

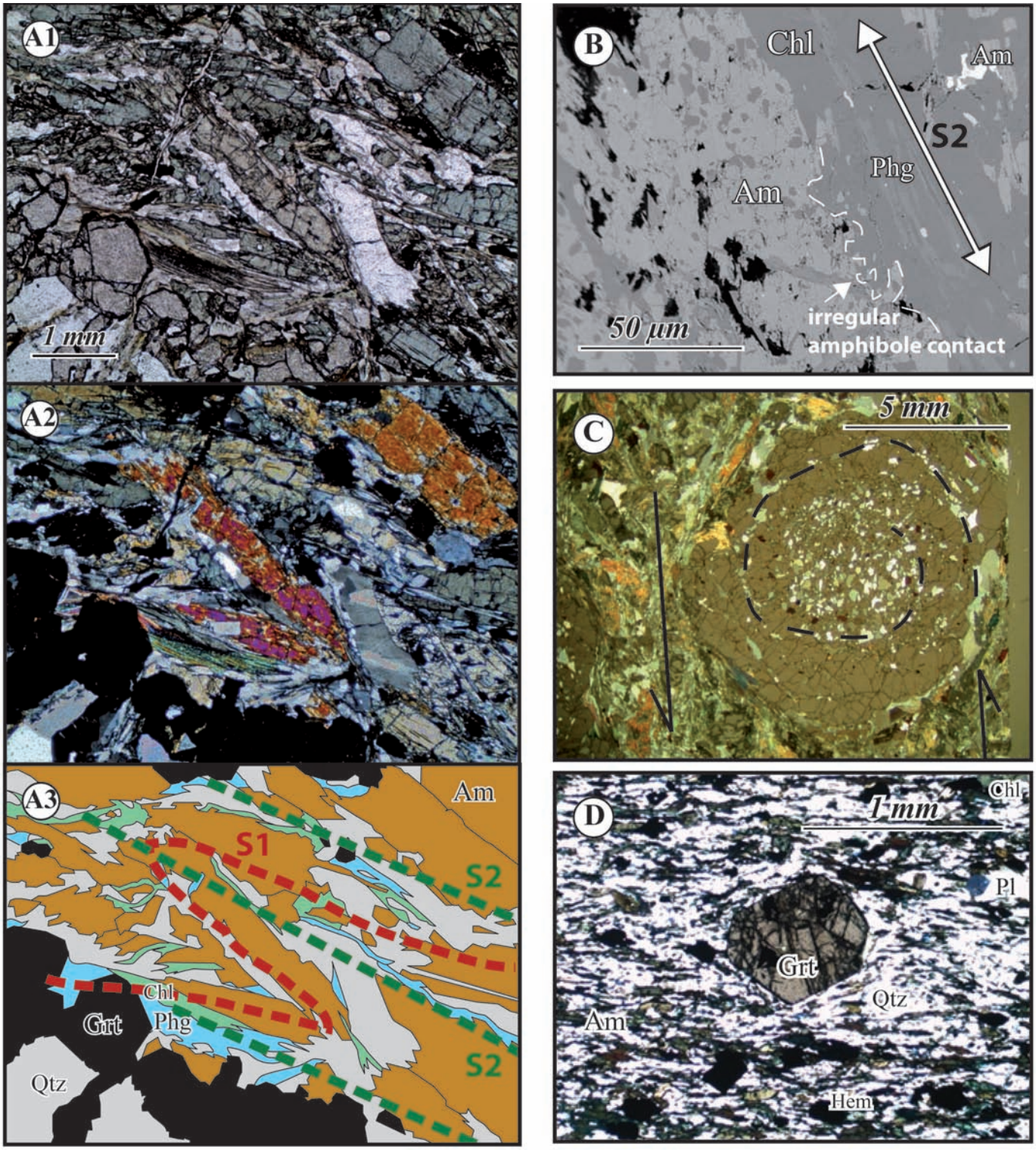

Fig. 7 - Micrographs of investigated Amasia (A-C) and Stepanavan (D) samples, and interpretative sketches. (A1) and (A2), micrograph of a thin section of garnet amphibolite sample AR-08-09c in plain and cross-polarized light, respectively. (A3), sketch of thin section photographs. Cross cutting relationships of amphiboles with micas (Phg) and chlorites (Chl) indicate the existence of amphiboles (Am) prior to micas. This is also supported by the garnets (Grt) and amphiboles, which are molded by micas and chlorites. The folded pattern of amphiboles defines a first foliation S_1 that is overprinted by the chlorite-phengite S_2, which appears to be in the axial planes of the folds drawn by the S_1 foliation. (B), back-scatter image of garnet amphibolite sample AR-09-08. Lineation is exhibited with the alignment of amphiboles, white micas and chlorites. (C), micrograph of garnet amphibolite sample AR-09-09. The garnet has a 'snowball' shape, and is rolled in response to syn-kinematic growth during shearing. (D), micrograph of eclogite sample ARM-11-13 from Stepanavan.

3 - In both localities, these two units are thrust on top of a southern (third) unit comprising brecciated basalts overlain by Early Cretaceous limestones, unconformably covered by a Late Paleocene flysch grading up into Early Eocene limestones and Mid- to Late Eocene volcanogenic deposits.

This structure in the Stepanavan area gives timing for final collision of SAB and Eurasia before the Late Paleocene, a little older than recorded in the rest of the Lesser Caucasus (before late-Middle Eocene; see Sosson et al., 2010). Ongoing post-collisional magmatism is represented by a Miocene to Quaternary volcanic cover sealing the nappe-stack.

GEOCHEMISTRY OF OPHIOLITIC ROCKS

The results of the analyzed samples of Amasia and Stepanavan ophiolites are coherent with all of the other ophiolites of the SAB, namely Sevan and Vedi, as well as with those of the Northeastern Anatolia (i.e. Refahiye, Şahvelet and Karadağ; Parlak et al., 2013). They all originate from a singular and intact section of oceanic crust, as they are all described as Lherzolite Ophiolite Type (LOT) with comparable petrological and geochemical compositions (Hässig et al., 2013a; 2013b; 2017). The different ophiolites outcrops are thus interpreted as the result of one major obduction event (Galoyan et al., 2009; Robertson et al., 2013; Hässig et al., 2017). Analytical procedures can be found in Supplementary Data S1.

Here, we present new data concerning the Stepanavan and Amasia ophiolites and the related metamorphic rocks. Analyses were segregated into two groups: (1) magmatic rocks (basalt, gabbro and plagiogranite) of preserved ophiolite units and (2) metamorphic rocks from the sub-ophiolitic units, which led to the identification of two distinct geochemical tendencies described below (Fig. 8; Table 1).

Supra-subduction tholeiitic signature

A tholeiitic (MORB-type) affinity is identified for the gabbro samples with a less marked fertile contamination, in comparison to some basalt samples. The variations in trace elements are indicative of a supra-subduction environment (Fig. 8). Negative Eu and Ti anomalies with relative Nb-Ta depletion are interpreted as resulting from the melting of a mantle source contaminated by subduction fluids. The ophiolite assemblages indicate that they derived from an oceanic crust in a back- or fore-arc basin position.

Similarly to those unmetamorphosed ophiolitic rocks, the analyzed Stepanavan blueschist from the sub-ophiolitic metamorphic rocks has a tholeiitic affinity, mainly characterized by enrichments in LILEs (e.g., Ba, Th, U) and negative Nb, Zr, and Sr anomalies which also resemble those of subduction-related arc volcanics (Perfit et al., 1980; Pearce et al., 1984). It is thus possible that these amphibolites derive from the ophiolite itself, thus sharing a common origin as the ophiolite.

Alkaline signature

A second affinity was found in rocks with an alkaline basalt composition (i.e. Hässig et al., 2013b) (Fig. 8B). The garnet-bearing amphibolites of Amasia and blueschists of Stepanavan have a similar composition as alkaline basalts, which may suggest a similar origin. Plotted in the Zr/Ti vs. Nb/Y Pearce diagram (Fig. 8C) these metamorphic rocks are consistent with an OIB signature. In particular, the samples show well-marked depletions in HREE (Figs. 8D1 and 8D2), which are ascribed to a source containing garnets (e.g., Rollinson, 1993).

The geochemical signature and the age of the Amasia ophiolites attest that they formed during the Jurassic in a fore- or back-arc supra-subduction marginal basin setting (Hässig et al., 2013a). Further, the similar ages and compositions concerning the obducted ophiolites onto the SAB strongly suggest that these are scattered relics of one major obduction event.

In N-MORB normalized multi-element spidergrams (Fig. 8D) the alkaline amphibolite and blueschist samples display patterns with enrichments in incompatible elements and slightly negative Nb and Sr anomalies. These patterns are consistent with those of typical ocean island basalts (Sun and McDonough, 1989). Such a setting has already been documented by Galoyan et al. (2007; 2009) and dated at 117 Ma for alkali pillow lavas in the Vedi area (Rolland et al., 2009b).

PETROGRAPHY AND MINERAL CHEMISTRY OF SUB-OPHIOLITIC METAMORPHIC ROCKS IN THE LESSER CAUCASUS

For the sub-ophiolitic unit of Amasia two mineral assemblages have been distinguished.

Previously, in Stepanavan three mineral assemblages have been recognized in the sub-ophiolitic blueschist unit ascribed to HP-LT (High Pressure-Low Temperature), LP-MT (Low Pressure-Mid Temperature), and LP-LT (Low Pressure-Low Temperature) conditions (Rolland et al., 2009a). In addition to these existing parageneses, a forth mineral assemblage has been identified (HP-HT).

Amasia sub-ophiolitic metamorphic unit

Two mineral assemblages have been identified in the garnet-bearing amphibolites after optical microscope observations (Fig. 7). They are: (1) an amphibolite facies assemblage (amphibole+plagioclase+garnet), and (2) a greenschist facies assemblage (white mica+chlorite). In the following sections, mineral name abbreviations follow Whitney and Evans (2010). Analytical procedures are described in Supplementary Data S7.

Amphibolite facies assemblage

The main metamorphic assemblage found in garnet-amphibolite unit is characterized by garnet, amphibole, rutile, plagioclase, ilmenite and quartz which underline the main foliation S_1 (Fig. 7).

Garnet grains are poikiloblastic, millimetre to centimetre in size, containing inclusion trails of quartz and amphibole arranged along a ‘snow-ball’ spiral pattern (Fig. 7C). Garnets are anhedral and intensely fractured. The fractures and rims are filled and moulded by white mica and chlorite, which recrystallize along a S_2 foliation (Figs. 7A and 7B). Microprobe analyses (Supplementary Data S2; Fig. 9A) show that garnets are solutions of almandine (57.8 to 68.6%), pyrope (8.1 to 32.9%), grossular (7.3 to 27.6%) and spessartine (0.05 to 5.1%) end members. Two tendencies have been identified: low pyrope (samples AR-08-09c and AR-09-09) and low grossular compositions (sample AR-09-08). Garnets are not chemically zoned (Fig. 9B). Instead they show a snowball pattern (Fig. 7C), which is a sign of their syn-kinematic growth during simple shearing, coeval with amphibole S_1 foliation.

Table 1 - Representative whole-rock analyses of samples from ophiolitic complex of Amasia.

ocality	Amasia												Stepanavan													
ample	AR-09-03	AR-09-14	AR-10-12	AR-08-13	AR-08-22	AR-08-29	AR-09-12	AR-09-17	AR-09-02	AR-08-09c	AR-09-06	AR-10-13	AR-03-53	AR-04-05	AR-04-20	AR-04-30	AR-04-32	AR-04-40A	ARM-11-01	ARM-11-02	ARM-11-06	AR-04-16	AR-04-45D	AR-11-08	ARM-04-44	ARM-11-10	ARM-11-13
rmation	Basalt	Basalt	Basalte	Gabbro	Gabbro	Gabbro	Gabbro	Gabbro	Plagiogranite	Garnet Amphibolite	Garnet Amphibolite	Garnet Amphibolite	Basalt	Basalt	Basalt	Basalt	Basalt	Basalt	Basalt	Basalt	Basalt	Gabbro	Gabbro	Gabbro	Plagiogranite	Blueschist	Eclogite
SiO2	50.18	51.98	58.85	54.68	55.90	47.73	56.91	47.81	72.70	54.37	46.09	45.23	50.93	52.50	53.30	51.95	50.91	53.81	68.95	55.04	67.14	48.60	55.52	46.83	76.86	47.88	56.98
TiO2	2.39	3.04	0.52	0.24	0.95	2.45	0.93	0.57	0.65	0.98	3.00	1.64	2.77	3.55	1.68	1.16	0.89	1.16	0.78	1.01	0.74	1.21	0.17	0.08	0.11	2.50	1.36
Al2O3	15.36	14.36	18.47	20.44	15.85	14.21	15.65	15.45	10.19	19.43	14.06	18.31	15.75	14.54	15.19	14.22	19.19	17.08	11.96	17.64	15.66	14.79	14.45	22.01	12.44	17.75	15.16
Fe203	1.95	1.76	0.99	0.88	1.72	2.10	1.67	1.32	0.79	1.73	1.88	1.92	1.99	2.15	2.30	1.39	1.58	1.43	0.83	1.71	0.83	1.99	1.38	1.30	0.41	1.43	1.97
FeO	9.93	8.97	5.05	4.51	8.76	10.72	8.53	6.74	4.03	8.83	9.59	9.78	10.15	10.99	11.72	7.10	8.07	7.29	4.22	8.72	4.25	10.14	7.05	6.63	2.11	7.27	10.04
MnO	0.19	0.22	0.16	0.10	0.17	0.15	0.17	0.16	0.10	0.13	0.09	0.20	0.28	0.25	0.24	0.16	0.16	0.16	0.11	0.19	0.08	0.21	0.16	0.13	0.03	0.12	0.24
MgO	3.63	4.12	2.52	5.36	5.02	6.35	5.11	7.99	2.22	3.65	2.38	7.38	4.46	3.42	4.29	7.34	5.44	3.82	2.63	3.95	3.35	9.36	8.06	9.84	0.79	4.96	3.44
CaO	9.27	11.69	7.27	9.79	5.81	11.66	4.95	19.42	5.93	6.34	15.08	15.36	5.59	6.12	5.03	11.23	8.54	9.86	6.44	4.93	0.82	10.42	7.20	10.17	2.09	11.00	3.46
Na2O	3.66	2.56	4.02	3.75	5.57	4.05	5.04	0.42	2.09	3.12	4.54	1.62	4.12	5.34	5.93	5.07	4.52	3.83	2.06	5.65	6.57	3.01	3.45	1.60	5.13	4.19	7.10
K2O	2.91	0.85	1.91	0.23	0.19	0.31	0.93	0.07	1.20	1.35	2.49	0.47	2.83	0.44	0.18	0.25	0.54	1.34	1.86	0.98	0.41	0.20	2.50	1.41	0.00	2.17	0.16
P2O5	0.55	0.45	0.24	0.01	0.05	0.28	0.10	0.05	0.09	0.06	0.79	0.17	1.13	0.70	0.13	0.12	0.15	0.22	0.15	0.18	0.14	0.07	0.06	0.00	0.02	0.73	0.11
Total	100.00	100.00	99.99	100.00	100.00	100.00	100.00	100.00	100.00	100.00	100.00	102.09	100.00	100.00	100.00	100.00	100.00	100.00	100.00	100.00	99.99	100.00	100.00	100.00	100.00	100.00	100.00
Ba	315.90	304.90	683.40				93.91	7.12	122.40		157.00		578.30	156.60	19.58	21.73	133.90	239.10	194.90	217.60	59.84	32.71	228.10	170.70	20.58	442.10	23.21
Rb	61.18	9.98	44.23				6.43	0.81	36.88		66.02		33.17	7.62	1.40	7.94	9.61	18.12	58.43	16.52	13.79	1.12	30.17	27.25	0.58	46.43	0.59
Sr	115.50	407.20	732.60				122.70	82.16	62.92		287.50		322.60	198.80	61.01	95.70	520.30	303.80	110.70	327.30	55.01	125.40	213.40	449.00	91.04	445.20	56.81
Ta	3.03	2.38	0.40				0.20	0.04	0.83		2.66		4.20	3.24	0.13	0.15	0.17	0.18	1.05	0.26	0.96	0.08	0.21			4.71	0.11
Th	3.83	2.36	5.77				0.65	0.13	6.46		2.95		5.98	4.66	0.43	0.19	0.72	1.46	8.10	1.64	10.02	0.18	1.28	0.04	0.02	7.58	0.38
Zr	204.70	176.80	120.90				52.50	30.50	194.30		201.40		294.40	373.50	86.00	68.43	44.40	99.18	175.40	89.06	174.30	42.74	21.26		6.48	238.40	65.41
Nb	40.52	30.76	5.82				2.38	0.45	9.89		35.66		57.95	42.33	1.62	1.90	2.14	2.29	12.58	3.19	11.15	1.01	2.14		0.35	66.57	1.31
Y	21.23	27.02	16.04				20.76	14.68	17.05		29.86		44.41	51.24	35.91	26.52	16.00	24.40	20.02	23.02	22.18	20.91	5.79	0.93	1.24	25.32	25.93
Hf	4.55	4.17	2.99				1.51	1.07	5.01		4.67		6.51	8.01	2.54	1.83	1.25	2.69	4.50	2.50	4.48	1.21	0.63	0.05	0.15	5.10	1.93
V	187.40	244.10	110.60				286.80	240.10	75.58		294.40		94.35	201.60	459.80	305.40	241.50	279.10	81.88	261.40	95.65	324.70	94.47	141.90	30.74	177.60	358.40
Cr	83.64	44.39	6.34				13.24	77.09	169.50				25.77		99.23	316.70	21.05	31.91	92.19	14.11	114.40	236.40	324.20	17.38	421.50	122.40	19.39
Ni	62.66	50.84	5.07				23.62	65.31	50.63		25.47		0.00		22.76	109.10	15.55	22.38	41.04	18.53	60.48	78.00	101.70	31.01	24.86	127.00	14.30
Co	19.96	31.08	13.83				30.39	35.43	8.97		32.74		16.75	31.93	38.85	42.98	29.51	29.05	9.33	24.56	16.86	51.46	31.50	47.56	7.71	37.25	30.97
U	0.86	0.52	2.13				0.22	0.06	1.51		0.91		1.46	1.20	0.12	0.09	0.19	0.67	1.93	0.36	2.32	0.06	0.43		0.01	2.21	0.13
Cu	8.10	61.91	31.48				37.35	10.59	13.48		41.51		9.48	14.94	64.58	132.80	12.60	188.10	18.94	65.07	47.35		189.90	69.90	189.50	49.75	31.80
Zn	79.63	87.58	70.12				42.99	63.26	57.65		154.90		137.10	152.70	130.60	81.13	150.90	86.53	71.52	117.90	76.51	60.28	60.33	45.07	23.13	87.01	110.80
Pb	4.89	3.59	7.62						11.91		3.96		2.54	2.24	2.29	1.93	7.22	3.42	5.80	5.94	3.25		3.61			3.42	2.44
Cs	1.73	0.21	0.48						1.17		2.03		0.49	0.14		0.68	0.97	0.60	1.77	0.27	0.60		0.00	0.90		1.06	
La	28.78	24.98	27.03				3.83	1.32	21.08		32.08		50.59	40.02	4.23	2.53	4.93	7.87	25.86	7.85	37.52	2.40	3.07	0.13	2.42	51.32	3.34
Ce	60.41	50.84	47.78				8.89	4.06	41.27		64.86		107.00	85.12	11.08	7.37	11.46	18.51	54.11	17.19	70.97	6.37	6.28	0.30	3.90	95.26	8.67
Pr	7.15	6.24	5.36				1.29	0.68	4.69		7.85		12.97	10.85	1.88	1.31	1.74	2.69	5.69	2.35	7.13	1.08	0.65	0.04	0.42	9.52	1.38
Nd	27.76	26.07	19.88				6.33	3.65	17.45		31.64		53.32	45.27	9.88	7.04	8.35	12.58	23.74	11.36	28.78	5.76	2.30	0.23	1.58	38.75	8.05
Sm	5.62	6.00	3.80				2.07	1.26	3.53		6.87		11.26	10.35	3.44	2.55	2.36	3.47	4.65	3.14	5.36	2.09	0.49	0.11	0.29	7.07	2.76
Eu	1.83	2.05	1.19				0.74	0.51	0.73		2.22		4.08	3.39	1.28	0.99	0.94	1.13	0.89	0.96	1.27	0.96	0.19	0.06	0.35	2.25	0.98
Gd	5.03	5.68	3.15				2.70	1.82	3.11		6.62		10.41	10.30	4.69	3.49	2.60	3.89	3.92	3.55	4.57	2.98	0.55	0.17	0.24	6.17	3.72
Tb	0.74	0.89	0.47				0.48	0.34	0.51		0.97		1.53	1.63	0.87	0.65	0.45	0.65	0.61	0.59	0.69	0.53	0.10	0.03	0.04	0.88	0.65
Dy	4.04	5.17	2.71				3.31	2.31	3.06		5.57		8.69	9.50	5.93	4.34	2.80	4.09	3.58	3.79	4.07	3.53	0.81	0.24	0.22	4.89	4.27
Ho	0.75	0.97	0.53				0.73	0.52	0.60		1.04		1.57	1.81	1.28	0.93	0.57	0.85	0.70	0.81	0.79	0.74	0.19	0.06	0.05	0.90	0.92
Er	2.01	2.50	1.55				2.14	1.55	1.73		2.78		4.16	4.93	3.79	2.75	1.63	2.46	2.00	2.34	2.20	2.15	0.65	0.17	0.15	2.43	2.66
Tm	0.29	0.35	0.24				0.33	0.24	0.26		0.39		0.57	0.70	0.58	0.42	0.24	0.38	0.31	0.36	0.33	0.32	0.12	0.03	0.03	0.33	0.41
Yb	1.83	2.24	1.70				2.25	1.67	1.81		2.48		3.64	4.51	3.89	2.84	1.60	2.54	2.09	2.39	2.24	2.10	0.91	0.19	0.21	2.24	2.74
Lu	0.28	0.33	0.26				0.36	0.27	0.28		0.37		0.56	0.69	0.61	0.44	0.25	0.39	0.32	0.38	0.35	0.32	0.17	0.03	0.04	0.34	0.43

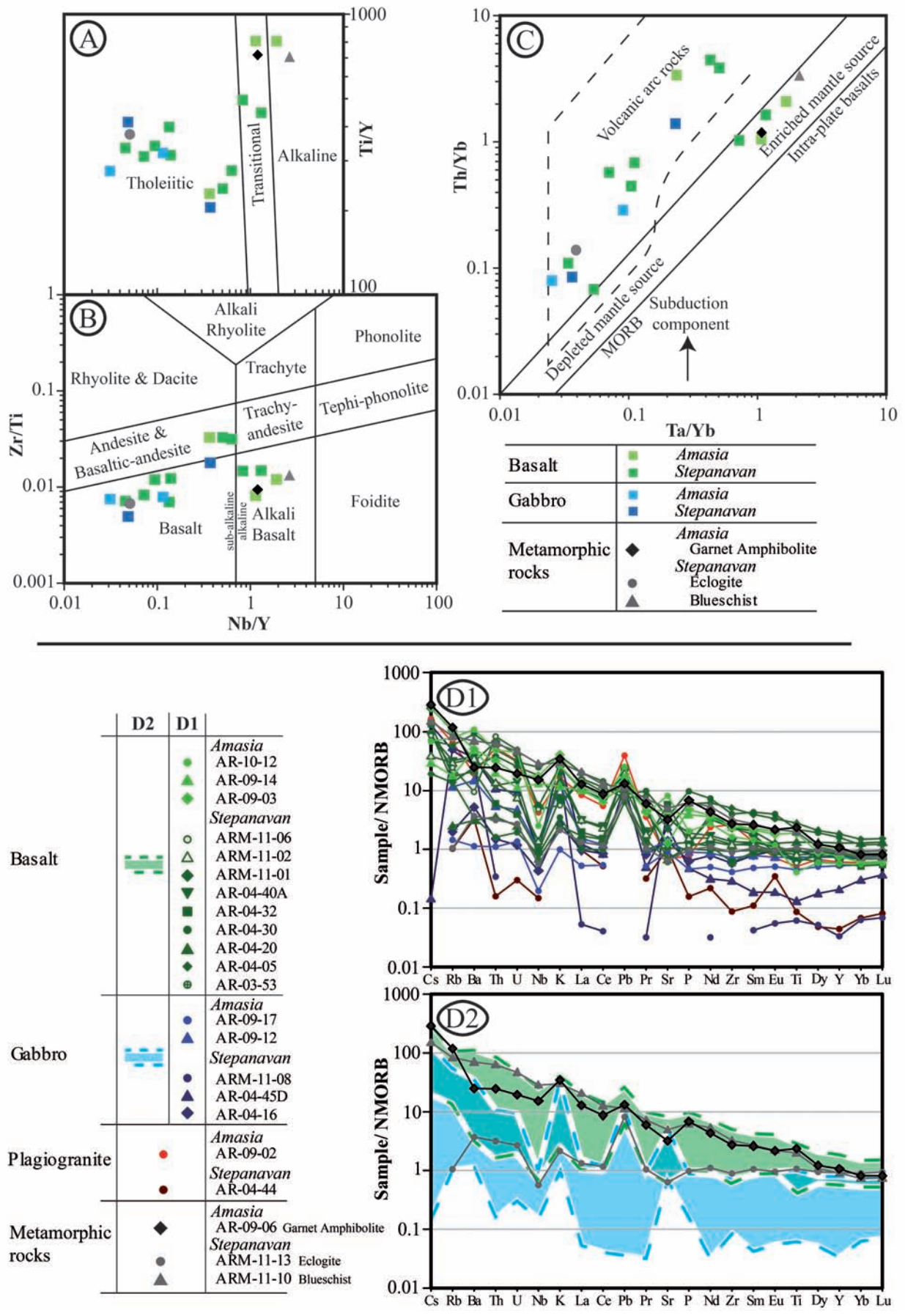

Fig. 8 - Geochemical diagrams of Amasia and Stepanavan ophiolitic rocks, featuring their main geochemical tendency and source characteristics. (A), Ti/Y versus Nb/Y discrimination diagram (after Pearce 1982). (B), Zr/Ti versus Nb/Y rock classification diagram (after Pearce, 1996). (C), Ta/Yb versus Th/Yb diagram discrimination diagram (after Pearce, 1982). (D), N-MORB normalized multi-element spider diagrams. Normalizing values are from Sun and McDonough (1989). Compilation of analyses shown in Table 1.

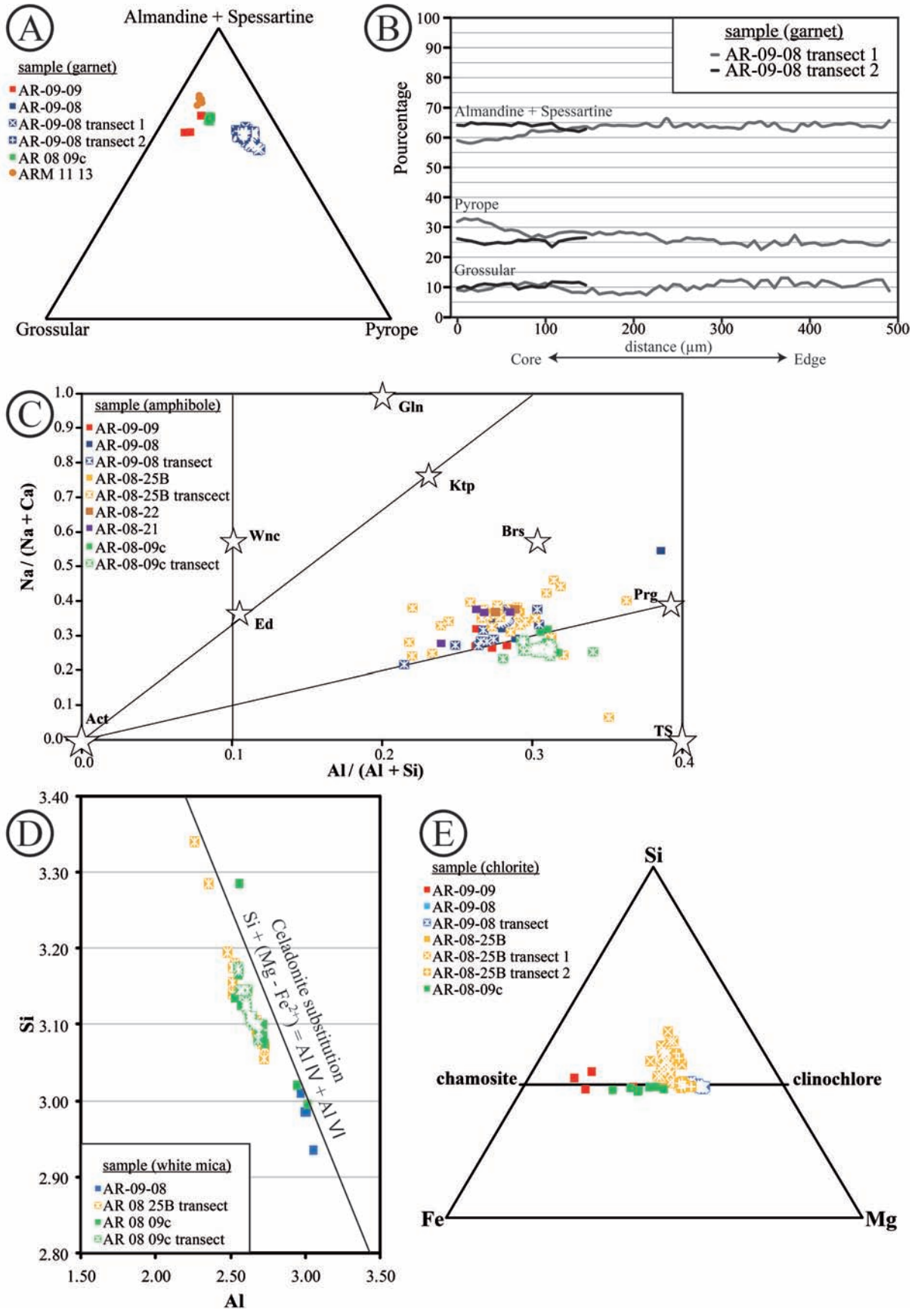

Fig. 9 - Diagrams of analyzed Amasia garnet amphibolite and Stepanavan eclogite minerals. (A), triangular plots showing chemical compositions of garnets. (B), compositional profiles of two garnets of the Amasia amphibolites. Note that the garnets are relatively homogenous in composition from core to rim. (C), Na/Ca+Na vs. Al/Al+Si ratios of amphiboles from amphibolite samples, abbreviations are according to Whitney and Evans (2010). (D), Si versus Al diagram for white micas from Amasia garnet amphibolite samples. (E), triangular plots showing chemical compositions of chlorites from Amasia amphibolite garnet amphibolite samples. Locations of samples are indicated on Fig. 4, as well as EPMA results in Supplementary Data S2, S3, S4, S5.

Amphiboles of the Amasia amphibolites mark the earlier S_1 foliation (Fig. 7A). They are fractured and have numerous fractures and irregular contacts with chlorite + phengite indicating their breakdown into these latter minerals (Fig. 7B). At the thin section scale, they are folded in isoclinal folds with axial planes parallel to the S_2 foliation marked by phengite + chlorite (Fig. 7A). Amphibole crystals are moulded as well as cross-cut by phengite and chlorite. They have fairly homogenous compositions (Supplementary Data S3; Fig. 9C). A slight increase of Fe and Ca to the detriment of Mg is observed from core to the mineral rims. The amphiboles observed are all high temperature type amphiboles, with intermediate compositions between barroisite, pargasite, tschermakite and edenite poles (Leake et al., 1997).

Rutile (< 1% vol.) is found in all the amphibolites. It is associated with amphiboles, garnets and plagioclases. They appear as inclusions but mainly in the S_1 foliation with elongated prismatic shapes and brownish colour in natural light. Using Back-Scattered Electron (BSE) imaging, no zoning is observed. Many of them have a dark aureole of ilmenite.

Plagioclase is scarce and of intermediate composition (between oligoclase and andesine).

Greenschist facies assemblage

The greenschist facies assemblage (or epidote amphibolite minerals) marks the S_2 foliation (Fig. 7), and thus constitutes a later metamorphic stage. It is characterized by the presence of chlorite, epidote and white mica. The chlorite, epidote and phengite most often cross-cut, wrap and mold amphibole and garnet (Figs. 7A, B).

The white micas are phengitic. They are intermediate solid solutions of muscovite and celadonite with a level of Si^{4+} substitution varying between 2.94 and 3.34 a.p.f.u. (atoms per formula unit) with a mean value of 3.12±0.07 a.p.f.u. (Fig. 9D; Supplementary Data S5). Massonne and Schreyer (1987) have shown that Si content of phengite increases progressively with pressure. Thus, these compositions agree with crystallization of the phengites during a relatively short stage of the P-T evolution as evidenced by the narrow spread in Si^{4+} substitution found in the analyses. Locally, paragonite is interlayered within phengite.

The analyzed chlorites (Supplementary Data S4) mostly range at intermediate X_{Fe} [Fe/(Fe + Mg)] contents ($0.57 < X_{Fe} < 0.78$) (Fig. 9E).

Stepanavan sub-ophiolitic metamorphic unit

Eclogite facies minerals

Metabasalt sample ARM-11-13 exhibits a garnet-chlorite-phengite-quartz-omphacite-hematite assemblage. The presence of omphacite indicates high pressure conditions.

Garnet grains are euhedral, slightly elongated along a well markedfoliation and intensely fractured (Fig. 7D). Microprobe analyses (Supplementary Data S2; Fig. 9A) show that garnets are homogeneous solutions of almandine (60.3 to 62.7%), pyrope (5.8 to 7.8%), grossular (16.9 to 19.2%) and spessartine (12.1 to 17.0%) end members. Their geometry suggests discreet low-angle rotation during syn-kinematic growth throughout simple shearing underlined by phengite. This would be coeval with phengite growth in relatively stable conditions.

PRESSURE-TEMPERATURE CONDITIONS OF THE STEPANAVAN AND AMASIA SUB-OPHIOLITIC METAMORPHIC UNITS

The P-T history is investigated using pseudosection modelling utilizing mineralogical and whole-rock composition of the samples ARM-11-13 and AR-08-09c of Stepanavan and Amasia sub-ophiolitic metamorphic units, respectively.

THERIAK-DOMINO pseudosection modelling

The pressure and temperature conditions of the amphibolite facies assemblage were inspected with pseudosection modelling performed in the Si-Al-Fe-Mg-Ca-Na-Ti-K-H_2O system and calculated with THERIAK-DOMINO (De Capitani and Petrakakis, 2010), using the internally consistent thermodynamic database of Bermann (1988) and Holland et Powell (1998). Figures 10 and 11 present P-T pseudosections of sample AR-08-09c (Amasia) and sample ARM-11-13 (Stepanavan) constructed using whole rock composition (Supplementary Data S6 and S7), respectively.

In order to further constrain the P-T evolution of metamorphic units, garnet composition isopleths for Stepanavan and garnet composition along with per formula units (a.p.f.u.) of X_{Fe} in chlorite and Si in phengite isopleths for Amasia were plotted (Supplementary Data S4 and S5).

Amasia sub-ophiolitic metamorphic unit

Amphibolite facies

For the first stage of metamorphism of this unit, the calculated field (garnet-amphibole-feldspar-biotite-quartz-ilmenite-magnetite) which best matches the paragenesis observed in sample ARM-08-09c is $4 \leq P \leq 8$ kbar and $550°C \leq T \leq 700°C$ (Fig. 10). Biotite was not directly observed, yet chlorite resulting from retromorphosis and alteration of biotite is visible. The calculated field is further constrained using garnet compositions. The intersection of the 0.65 and 0.7 almandine, with 0.17 and 0.19 grossular, and 0.13 pyrope isopleths corresponds to the measured proportions in garnet composition in sample AR-08-09c (approximately 67% almandine, 18% de grossular 13% pyrope). This new field is bounded to P = 6.5±0.5 kbar and T = 600±20°C (Fig. 10). These amphibolite facies conditions correspond to the first and main stage of metamorphism recorded in garnet amphibolites.

Greenschist facies

The second (greenschist facies) stage of metamorphism of the Amasia sub-ophiolitic metamorphic unit corresponds to the calculated P-T field featured by the feldspar-ilmenite-chlorite-phengite-clinozoisite-epidote-quartz assemblage, which best matches the second paragenesis observed in ARM-08-09c. Yet, the absence of clinozoisite or epidote in the sample may be due to its presence in very small quantities, as it was observed in other thin sections of this outcrop. This calculated field is of $1.25 \leq P \leq 4.5$ kbar and $320°C \leq T \leq 380°C$ (Fig. 10). This field is further constrained using X_{Fe} and Si isopleths corresponding to chlorite and phengite, respectively, in sample AR-08-09c. The intersection of the 0.5 X_{Fe} chlorite with the 3.14 Si phengite isopleths indicates a restrained field of P = 2.5±1 kbar and T = 350±30°C (Fig. 10).

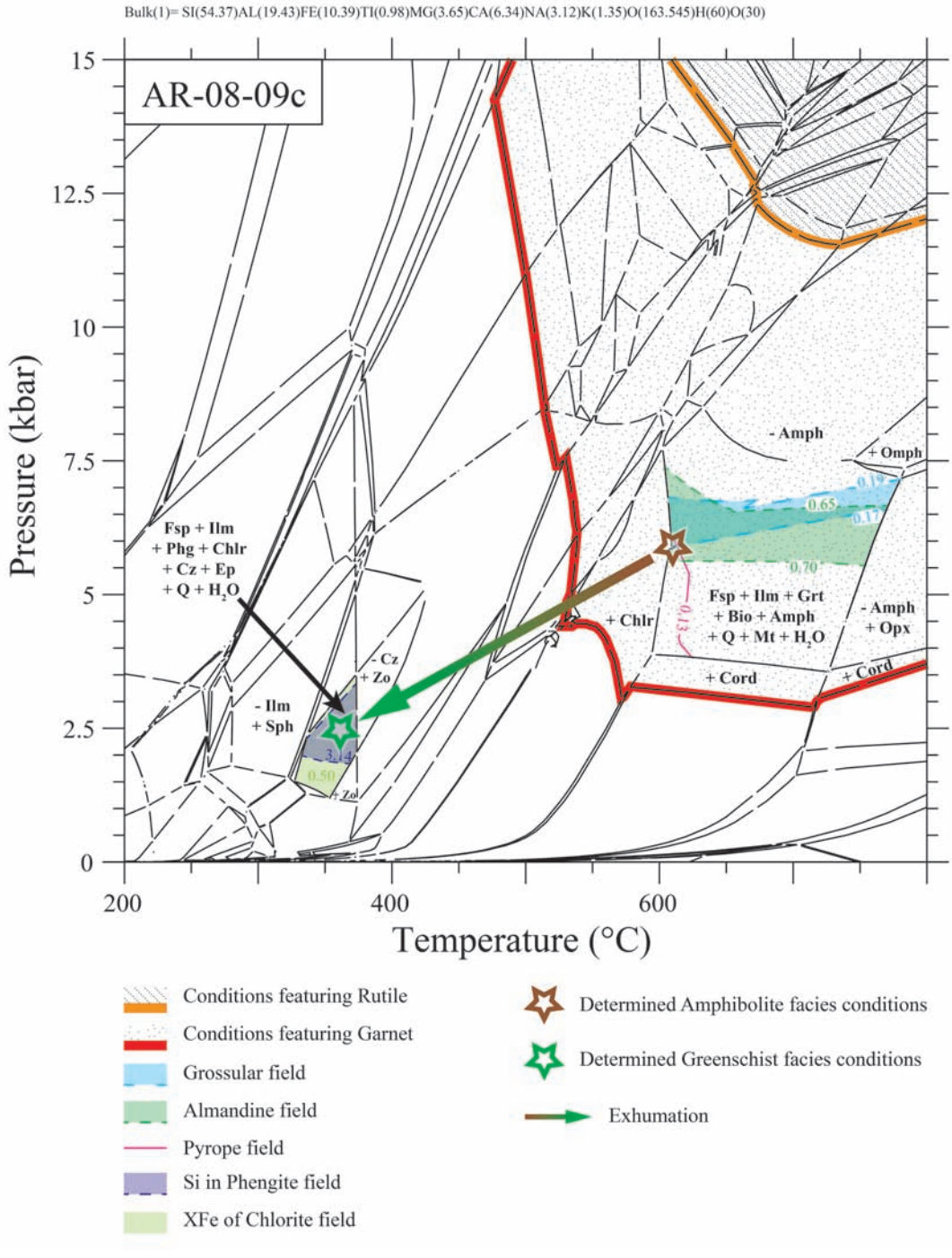

Fig 10 - Pseudosection computed for the Si-Al-Fe-Mg-Ca-Na-Ti-K-H_2O system calculated with THERIAK-DOMINO (De Capitani and Petrakakis, 2010) for sample AR-08-09c. The domain corresponding to observations and results of mineral analyses is indicated with brown and green stars for amphibolite and greenschist facies conditions, respectively. Detailed results in Supplementary Data S6.

Stepanavan sub-ophiolitic metamorphic unit

The calculated P-T field featured by the garnet-omphacite-chlorite-phengite-kyanite-quartz-hematite-H_2O assemblage, which best matches the paragenesis observed in ARM-11-13 is 17.5 ≤ P ≤ 20 kbar and 550°C ≤ T ≤ 600°C (Fig. 11). Even if kyanite has not been directly observed in ARM-11-13, aluminium silicates modelled in THERIAK-DOMINO generally correspond to excess alumina that may be contained in other silicates. This field is further constrained using garnet compositions. The intersection of the 0.6 almandine isopleth with the 0.16 and 0.18 grossular isopleth corresponds to the measured proportions in garnet composition in sample ARM-11-13 (approximately 60% almandine and 17% grossular). This new field is bounded to P = 18.5±0.2 kbar and T = 590±5°C (Fig. 11). These HP-HT conditions validate the classification as eclogite facies and must be implemented in pre-existing P-T diagrams for this sub-ophiolitic metamorphic unit.

RADIOMETRIC DATING

Dating of the Amasia sub-ophiolitic metamorphic unit was undertaken by two methods. Single-grain laser $^{40}Ar/^{39}Ar$ dating was carried on amphiboles and white micas. LA-ICP-MS on single grains of rutile was used for U-Pb dating. Analytical procedures are presented in Supplementary Data S1. Detailed dating results are displayed in Supplementary Data S8, S9, S10, S11 and S12.

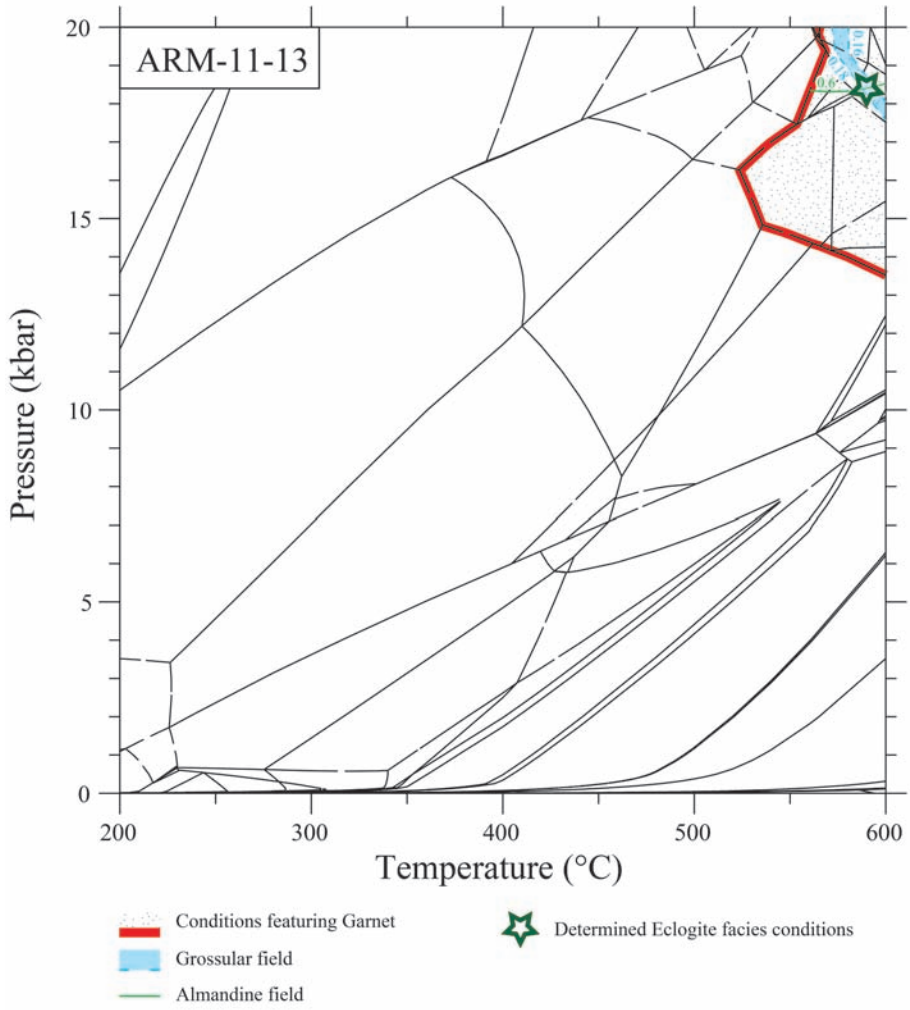

Fig 11. - Pseudosection computed for the Si-Al-Fe-Mg-Ca-Na-Ti-K-H2O system calculated with THERIAK-DOMINO (De Capitani and Petrakakis, 2010) for sample ARM-11-13. The domain corresponding to observations and results of mineral analyses is indicated with green star for eclogite facies conditions, respectively. Detailed results in Supplementary Data S7.

Dating of amphiboles

One amphibole from sample AR-09-08 (K390) yielded a plateau age of 87.7±2.8 Ma (MSWD of 0.06) (Fig. 12A), computed with the major last three heating steps (which form 94.7% of the released ^{39}Ar). For a matter of validation, the inverse isochron age is 86.0±7.0 Ma (MSWD of 0.02), in agreement with the plateau age.

One amphibole from sample AR-09-15 (K402) yielded a plateau age of 91.2±1.6 Ma with a MSWD of 0.59 (Fig. 12B) computed with six out of seven heating steps pertaining 98.0% of total released ^{39}Ar. The inverse isochron age is 89.3±3.8 Ma (1σ) with a MSWD of 0.74, which is in good agreement with the plateau age.

One amphibole from the sample AR-08-09c (K427) yielded a plateau age of 90.3±1.5 Ma (MSWD of 0.01) (Fig. 12C) computed with the last five heating steps representing 92.8% of total released ^{39}Ar. In this sample, the inverse isochron age is 90.2±1.9 Ma with a MSWD of 0.01, within error similar to the plateau age.

In conclusion, the three ^{40}Ar/^{39}Ar amphibole ages are similar within error. They agree with a common crystallization age during the amphibolite HT peak at about 90±0.5 Ma.

Dating of phengites

The phengite separated from the sample AR-08-09c (K428) yielded a plateau age of 89.7±0.7 Ma (MSWD of 0.80) (Fig. 12D) computed with the last seven heating steps representing 97.0% of the total ^{39}Ar. The inverse isochron overlaps within 1σ error the plateau age.

This age indicates that the MP-MT phengite-chlorite paragenesis age is similar within error to the amphibolite HT peak age obtained above, and likely occurred around 90 Ma.

In conclusion of the ^{40}Ar/^{39}Ar dating section, the amphibole and phengite ^{40}Ar/^{39}Ar ages obtained on Amasia amphibolites are similar within errors and they cannot definitively be distinguished. They agree with crystallization during a rapid metamorphic cycle related to oceanic crust obduction at about 89-90 Ma (Fig. 12E), at the beginning of the Late Cretaceous (Turonian). These data are consistent with palaeontological dating of sediment deposits directly under (Cenomanian, i.e. ≥ 93.9 Ma) or sealing (Coniacian-Santonian, i.e., ≤ 89.8 Ma), the obduction front of Armenian ophiolites (Sosson et al., 2010; Danelian et al., 2014).

Dating of rutile

The rutile was analyzed “in-situ” on a thin section cut in sample AR-09-15 following a procedure outlined in earlier reports (e.g., Bruguier et al., 2017) and described in more details in Supplementary Data S1. Fifteen analyses were performed on twelve grains chosen for the lack of ilmenite rims that often wrap the rutile. Analyzed grains have low U contents (from 0.4 to 3.4 ppm) and consequently very low

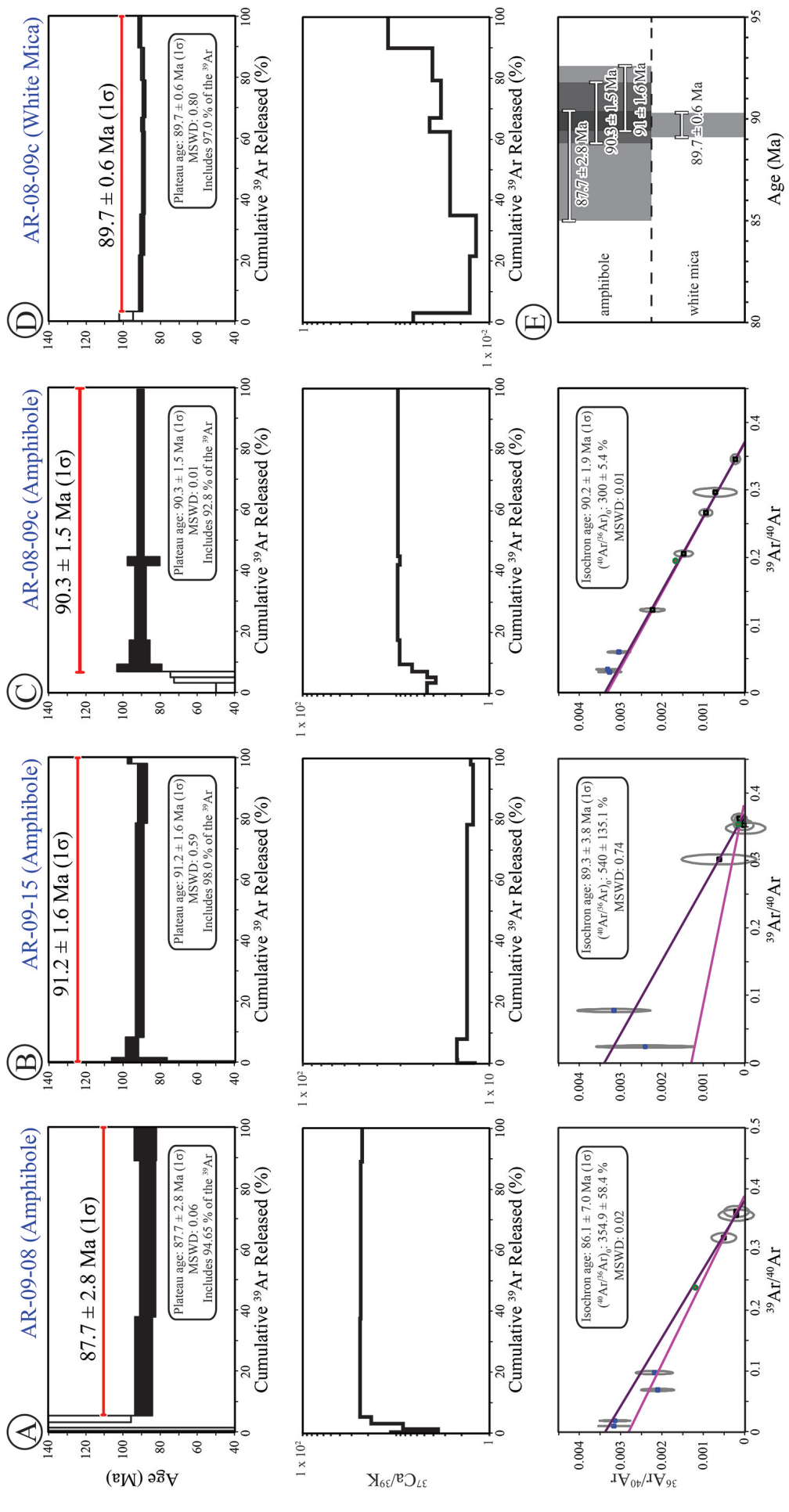

Fig. 12 - $^{40}Ar/^{39}Ar$ age, Ca/K spectra and inverse isochrons. (A), amphibole from sample AR-09-08. (B), amphibole from sample AR-09-15. (C), amphibole from sample AR-08-09c. (D), white mica from sample AR-08-09c. Locations of samples are shown on Fig. 4. (E), compilation of ages which is also shown in Table 2, as well as detailed dating results in Supplementary Data S8, S9, S10, S11.

Table 2 - $^{40}Ar/^{39}Ar$ dating results.

Step	Laser power (mW)	Atmospheric cont (%)	^{39}Ar (%)	$^{37}Ar_{Ca}/^{39}Ar_K$	$^{40}Ar^*/^{39}Ar_K$	Age (Ma ± 2σ)
Muscovite AR-08-09c, J = 0.02, plateau age: 89.7 ± 1.12 Ma (97 % ^{39}Ar) (MSDW: 0.80)						
1	400		3.01	0.06	2.95	98.38 ± 7.48
2	460		18.48	0.02	2.71	90.58 ± 1.99
3	493		13.40	0.01	2.68	89.72 ± 2.40
4	523		27.19	0.03	2.66	89.07 ± 1.75
5	544		4.55	0.04	2.67	89.51 ± 1.83
6	616		12.24	0.03	2.65	88.75 ± 1.76
7	695		10.69	0.04	2.68	89.57 ± 1.78
8	1111		10.43	0.11	2.72	91.04 ± 1.78
Amphibole AR-08-09c, J = 0.02, plateau age: 90.3 ± 3.04 Ma (92.7 % ^{39}Ar), inverse isochron age: 90.2 ± 2.0 Ma (MSDW: 0.01)						
1	450		3.49	4.65	0.25	8.65 ± ± 81.95
2	500		1.82	3.78	0.76	26.04 ± ± 92.44
3	552		1.89	4.60	1.52	51.53 ± ± 45.35
4	600		2.37	6.51	2.71	90.92 ± ± 24.05
5	651		7.92	8.92	2.71	90.76 ± ± 10.96
6	694		24.63	9.50	2.70	90.32 ± ± 6.01
7	726		2.81	8.74	2.64	88.64 ± ± 17.40
8	1111		55.06	8.87	2.69	90.24 ± ± 3.60
Amphibole AR-09-15, J = 0.02, plateau age: 91.2 ± 3.1 Ma (98.1 % ^{39}Ar), inverse isochron age: 89.3 ± 3.9 Ma (MSDW: 0.74)						
1	400		0.05	1.65	12.09	8.65 ± 81.95
2	600		0.25	11.73	0.74	26.04 ± 92.44
3	661		1.08	14.66	2.72	51.53 ± 45.35
4	720		6.76	14.59	2.84	90.92 ± 24.05
5	770		70.55	12.97	2.71	90.76 ± 10.96
6	820		19.62	12.02	2.66	90.32 ± 6.01
7	1111		1.69	12.49	2.88	88.64 ± 17.40
Amphibole AR-09-08, J = 0.02, plateau age: 87.7 ± 5.6 Ma (94.7 % ^{39}Ar), inverse isochron age: 86.1 ± 7.1 Ma (MSDW: 0.02)						
1	400		0.40	10.08	5.60	182.99 ± 390.11
2	500		0.98	3.58	3.33	110.98 ± 201.40
3	551		1.78	8.69	5.36	175.59 ± 54.69
4	601		2.19	19.33	3.55	117.94 ± 44.62
5	659		32.48	24.34	2.65	88.85 ± 9.37
6	712		51.42	24.01	2.58	86.66 ± 8.41
7	999		10.76	22.98	2.62	87.95 ± 11.82

radiogenic Pb, generally below 100 ppb (Table 3). Reported in a Tera-Wasserburg diagram (Fig. 13), all data points are aligned along a chord intersecting concordia at 90.2±5.2 Ma (2s) (MSWD = 1.7, n = 15). It is noteworthy that this age is very similar within errors to the amphibole and white mica $^{40}Ar/^{39}Ar$ ages obtained for this metamorphic unit.

DISCUSSION

The study of the metamorphic rocks found under the Eastern Anatolia-Armenia ophiolite nappe provides key data for the reconstruction of the obduction history in this region and may provide insights for the understanding of obduction processes (e.g., Wakabayashi and Dilek, 2000; 2003; Gaggero et al., 2009; Duretz et al., 2015). These sub-ophiolitic metamorphic units record variations in temperature and pressure of rocks dragged below the obducted ocean lithosphere, throughout processes ranging from intra-oceanic subduction to obduction due to the progression of a relatively cold sinking slab and hot overriding plate (e.g., Coleman, 1981; Hacker and Gnos, 1997; Agard et al., 2016). Descriptions of such units are widespread in Anatolia, to the west of the study area (Whitechurch et al., 1984; Robertson and Karamata, 1994; Sherlock et al., 1999; Abd El-Naby et al., 2000; Al-Riyami et al., 2002; Beccaletto and Jenny, 2004; Çelik et al., 2006; 2011; Plunder et al., 2015; 2016). These new finding in NW Armenia, extend the zone of sub-ophiolitic metamorphic units known metamorphic sole and others recording the history of the subduction of the Northern Neotethys to the east of Anatolia. With similar ages found along the Erzincan-Sevan Akera Suture, it appears that metamorphic soles recorded a major event of obduction occurring at c. 90 Ma. In the following discussion, we first discuss the meaning of the obtained P-T-t data. This leads us to reconstruct a 'most likely' P-T-t history of the metamorphic sole, sub-ophiolitic metamorphic units and the succession of geodynamic events. We further argue for the presence of a single and major ophiolite nappe in the Anatolia-Lesser Caucasus region, based on a comparison of geochemical along with mineral and geochronological data of the various ophiolitic outcrops, and propose a reconstruction of the obduction history in this region.

Table 3 - U-Pb laser ablation ICP-MS results.

sample	Pb* (ppm)	U (ppm)	$^{207}Pb/^{206}Pb$	(1σ)	$^{207}Pb/^{235}U$	(1σ)	$^{206}Pb/^{238}U$	(1σ)	rho	Apparent ages (Ma) $^{206}Pb/^{238}U$	(1σ)
AR-09-15											
ha1	0.026	0.47	0.381 ±	0.096	1.183 ±	0.342	0.0225 ±	0.0032	0.49	143.7	± 20.0
ha2	0.132	1.36	0.514 ±	0.059	1.902 ±	0.243	0.0269 ±	0.0015	0.44	170.9	± 9.4
ha3	0.083	2.80	0.094 ±	0.015	0.189 ±	0.032	0.0146 ±	0.0008	0.33	93.5	± 5.2
ha4	0.068	1.83	0.235 ±	0.051	0.435 ±	0.101	0.0134 ±	0.0010	0.33	86.1	± 6.6
ha5	0.021	0.42	0.287 ±	0.067	0.964 ±	0.261	0.0243 ±	0.0033	0.50	155.0	± 20.8
ha6	0.043	0.96	0.284 ±	0.054	0.769 ±	0.169	0.0196 ±	0.0021	0.49	125.4	± 13.4
ha7	0.028	0.70	0.281 ±	0.051	0.735 ±	0.158	0.0190 ±	0.0022	0.54	121.3	± 14.0
ha8	0.053	1.35	0.166 ±	0.031	0.386 ±	0.077	0.0168 ±	0.0010	0.31	107.6	± 6.5
ha9	0.009	1.00	0.097 ±	0.053	0.207 ±	0.115	0.0155 ±	0.0020	0.23	99.1	± 12.5
ha10	0.059	2.41	0.071 ±	0.027	0.138 ±	0.053	0.0141 ±	0.0009	0.18	90.1	± 6.0
ha11	0.019	0.78	0.241 ±	0.094	0.731 ±	0.296	0.0219 ±	0.0024	0.27	140.0	± 15.4
ha12	0.029	1.48	0.056 ±	0.089	0.098 ±	0.157	0.0127 ±	0.0014	0.07	81.5	± 8.6
ha13	0.105	3.39	0.074 ±	0.016	0.162 ±	0.035	0.0159 ±	0.0007	0.21	101.8	± 4.5
ha14	0.088	2.85	0.209 ±	0.039	0.417 ±	0.083	0.0144 ±	0.0010	0.34	92.5	± 6.2
ha15	0.095	2.25	0.320 ±	0.055	0.756 ±	0.135	0.0171 ±	0.0009	0.30	109.4	± 5.9

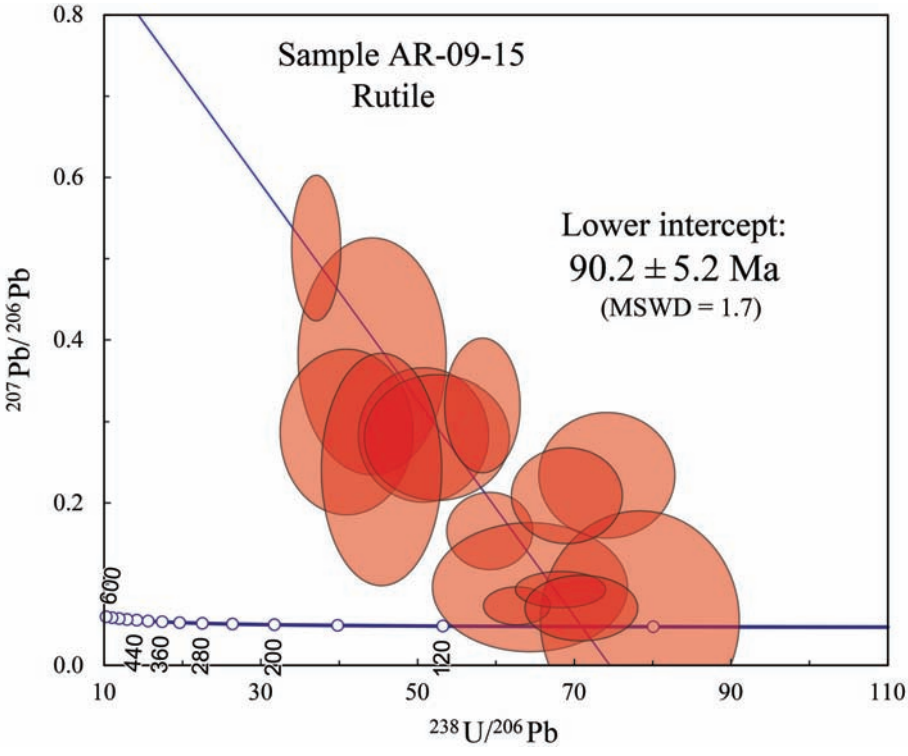

Fig. 13. U-Pb laser ICP-MS ablation Tera-Wasseburg concordia diagram for the sample AR-09-15. Compilation of ages is shown in Table 3. Location of the sample is shown on Fig. 5, as well as detailed dating results in Supplementary Data S12. Data-point error ellipses are 68.3% confidence.

Significance of the U-Pb and $^{40}Ar/^{39}Ar$ datings

The ages obtained in this paper are the first for the Amasia sub-ophiolitic metamorphic rocks and only the third for those of Stepanavan.

$^{40}Ar/^{39}Ar$ ages on amphibole and phengite may be related the crystallization history of these minerals during mineral prograde, metamorphic peak and retrograde phases of PT evolution (e.g., Warren et al., 2012; Uunk et al., 2018). P-T grids computed with THERIAK-DOMINO show that these minerals preserve stages (1) of the amphibolite facies temperature peak (amphibole), and (2) retrogression in the greenschist facies (phengite). For rutile, experimental studies (Cherniak, 2000; Vry and Backer, 2006) or natural examples (e.g., Kooijman et al., 2010; 2012; Gao et al., 2014) indicate closure temperature for Pb diffusion in the range 600-650°C. The estimated peak amphibolite metamorphic conditions of c. P = 6.5±0.5 kbar and T = 600±20°C are within the range of the closure temperature for rutile. Given that this mineral is found in the S_1 foliation, associated to syn-kinematic garnet, the rutile age of 90.2±5.2 Ma is attributed to peak amphibolite facies conditions. The estimated range for amphibole closure temperature (Tc ≈ 500°C; McDougall and Harrison, 1999) is very close to or slightly lower than peak amphibolite facies conditions, which leads to propose that the amphibole age reflects either the age of peak metamorphic conditions, or cooling through the amphibole closure temperature. It is noteworthy that the

$^{40}Ar/^{39}Ar$ amphibole ages and the U-Pb rutile age are similar within errors, whilst having distinct closure temperatures. In turn these ages are also similar to that determined on the phengite from sample AR08-09c, which is clearly attributed to S_2 and to the greenschist facies overprint. This implies that: (i) all ages reflect resetting of the U-Pb and Ar-Ar systems during retromorphosis due to fluid circulations (e.g., Tartèse et al., 2011), (ii) the ages reflect a crystallization of the two minerals at very close PT conditions, or (iii) a very rapid cooling process occurred.

The first hypothesis implies the resetting of the Ar-Ar (amphibole) and U-Pb (rutile) systems, which can be ascribed either to reheating above their respective closure temperatures or to recrystallization during fluid-assisted S_2 deformation. Reheating was not observed in the studied thin sections and it therefore discarded. Fluid assisted recrystallization would indeed yield similar U-Pb and Ar-Ar ages, yet rutile is thought to be robust to reset by fluids (e.g., Gasser et al., 2015). Further, such a process should be apparent not only in the geochronological data but also in the mineral geochemistry. Fluid assisted recrystallization is even more unlikely as in general a mineral zoning is observed in amphiboles that underwent such recrystallization (e.g., Villa et al., 2000), while dated minerals appear to be unzoned. Rutile exhibits ilmenite dark aureoles that indicate breakdown occurring during the retrograde stage of metamorphism, but U-Pb analyses of rutile were focussed on ilmenite-free portions of the crystals. Resetting of both Ar-Ar and U-Pb system during retrograde metamorphism and fluid assisted recrystallization is thus considered unlikely.

Considering the second hypothesis, we showed in section 5.2 that the PT conditions derived from the two (amphibolite and greenschist facies) parageneses, which crystallize with amphibole and phengite are significantly distinct (600±20°C for the crystallization of amphibole and 350±30°C for that phengite), therefore they are ascribed to two distinct steps in the PT path (Figs. 10 & 14).

The third hypothesis implies that the obduction process was very rapid. This possibility is in agreement with paleontological datings obtained from below (before) and above

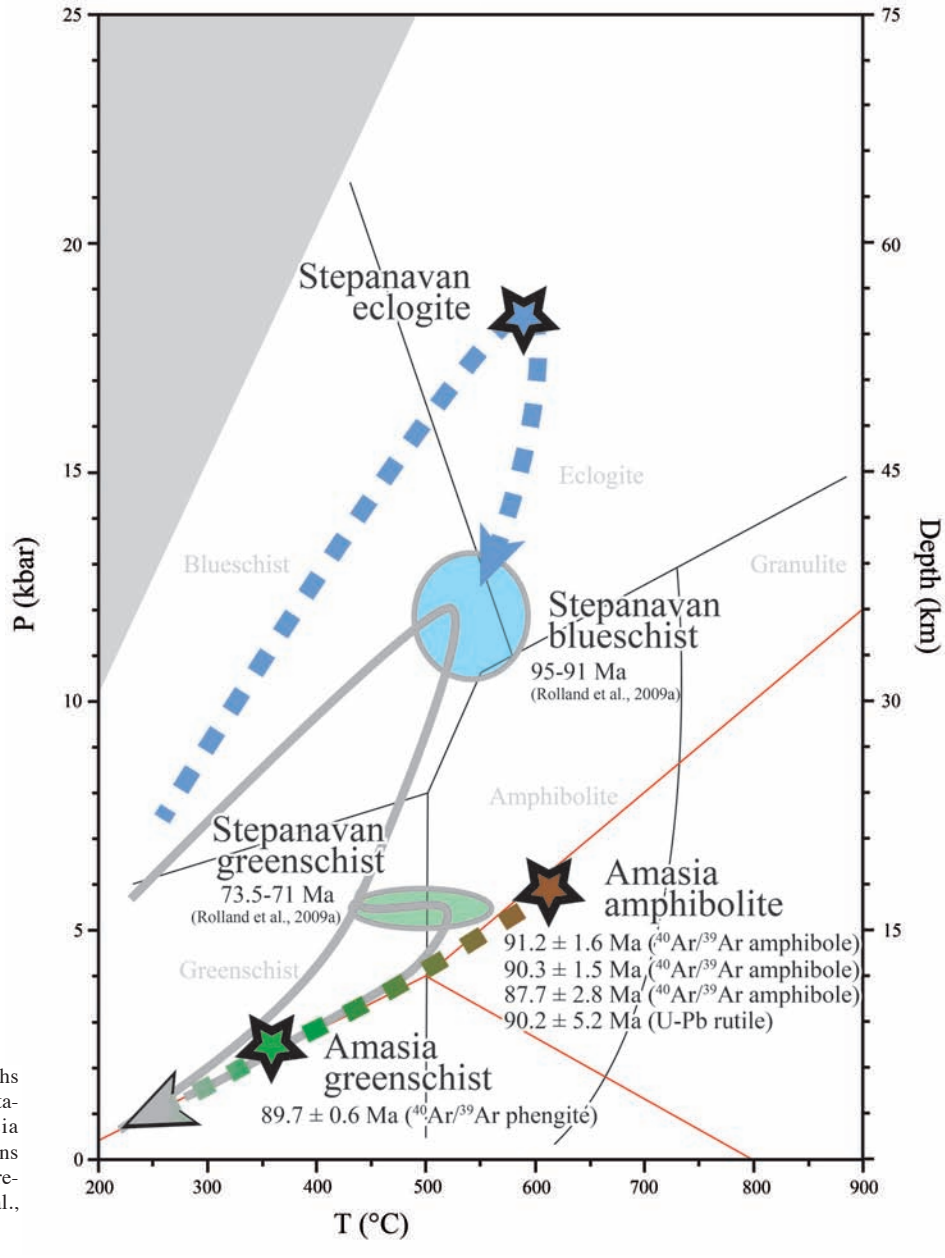

Fig. 14 - Compilation of determined P-T-t paths for the sub-ophiolitic Amasia-Sevan-Akera metamorphic rocks. Amasia amphibolite, Amasia greenschist and Stepanavan eclogite conditions are represented by brown, green and blue stars, respectively. Stepanavan blueschist (Rolland et al., 2009a) are represented in grey.

(after) the ophiolite nappe (Sosson, et al., 2010; Danelian et al., 2014), which constrain ophiolite emplacement directly after Cenomanian, i.e. ≤ 93.9 Ma, and just before the Coniacian-Santonian, i.e. ≥ 89.8 Ma. The paleontological indirect dating is thus similar, within error, to the $^{40}Ar/^{39}Ar$ and U-Pb ages. It is thus unlikely that the age of peak metamorphism could have been significantly older. Therefore, the metamorphism could be ascribed to the rapid emplacement of the ophiolite nappe in the Lesser Caucasus.

Significance of the P-T-t path

Amasia metamorphic sole

The sub-ophiolitic garnet-bearing amphibolites of Amasia provide invaluable insight into the early stages of obduction. The thermo-barometric estimates preformed on this lithology show a MP-HT peak (P = 6.5 kbar, T = 600°C) dated to c. 90 Ma by U-Pb dating on rutile and $^{40}Ar/^{39}Ar$ dating on amphibole. A second metamorphic stage has also been identified in this lithology, a LP-LT (P = 2.5 kbar, T = 350°C), with retromorphic greenschist facies dated at 89 Ma by $^{40}Ar/^{39}Ar$ on phengite. The MP-HT peak conditions imply a high thermal gradient (30°C/km) as well as overthrusting of a thinned oceanic lithosphere (20 km), which suggest an abnormally hot oceanic domain at obduction onset.

We propose that the MP-HT amphibolite paragenesis was likely formed throughout oceanic lithosphere overthrusting by intra-oceanic subduction in a hot (and thus young) oceanic domain. Indeed, the MP-HT conditions of the garnet-amphibolites are hypothesized to be due to the remanence of the significant heating (thermal rejuvenation) of the oceanic lithosphere following the emplacement of hotspot series (Rolland et al., 2009b). The first phase of deformation (S_1) and formation of amphibolite is thus ascribed to the initiation of this oceanic overthrusting in a back-arc domain within a relatively hot and thinned oceanic lithosphere ending with primary ophiolite emplacement.

The LP-LT greenschist paragenesis should have developed throughout further exhumation after the main obduction phase. The second phase of deformation (S_2) during this greenschist LP-LT stage marking the transition from primary ophiolite emplacement to exhumation and subsequent passive obduction by gravity sliding (Hässig et al., 2016a; 2016b; Lagabrielle et al., 2013).

These two P-T-t stages in the obduction metamorphic sole show that exhumation and subsequent passive obduction occurred within 1 Myr after the metamorphic peak, and feature a rapid obduction process.

Stepanavan sub-ophiolitic metamorphic unit

This study demonstrates the existence of a HP-HT (P = 18.5 kbar, T = 590°C) eclogite event evidenced at Stepanavan. This is the first time that an eclogite has been described in the Sevan-Akera suture zone. These rocks were sampled next to outcrops evidencing a blueschist facies metamorphism (P = 12 kbar, T = 550°C) dated at 94 Ma (Rolland et al., 2009). The conditions recorded by these rocks is ascribed to the metamorphism occurring during intra-oceanic Neotethyan north dipping subduction 5~10 Myr prior to, or may feature the early stages of, the obduction event. The P-T conditions of these rocks evidence burial to depths of 35 km and 55 km for the blueschist and eclogite units, respectively. The inferred thermal gradient for this subduction, with 15°C/km and 11°C/km for the blueschist and eclogite rocks, respectively, is abnormally hot compared to the typical 8~10°C/km (Gerya et al., 2002; Syracuse et al., 2010) or along the hotter limit for subductions of young oceanic lithosphere (Penniston-Dorland et al., 2015). A $^{40}Ar/^{39}Ar$ phengite age of 71-74 Ma (Rolland et al., 2009) of the third blueschist was associated to retromorphosis during exhumation of this unit.

A transition from subduction to obduction

Sub-ophiolitic metamorphic rocks scarcely outcrop along the Northern Neotethyan Suture in Northeastern Anatolia and Lesser Caucasus regions. Besides Stepanavan and Amasia localities, in Northeastern Turkey, near Erzincan the Yoncayolu Metamorphic Rocks (YMR; greenschist rocks consisting of chlorite schists, muscovite-chlorite schists and metabasic rocks) recorded P = 4 kbar and 320 ≤ T ≤ 350°C (chlorite geothermometry; Gucer and Aslan, 2014). $^{40}Ar/^{39}Ar$ dating on plagioclases from the metabasic samples of the YMR provides ages of 100.8±3.4 Ma and 94.1±3.3 Ma (Gucer and Aslan, 2011). This metamorphism is synchronous with the blueschists of Stepanavan. Geochemical volcanic-arc affinities of the YMR indicate that the protoliths developed in a volcanic-arc setting (Gücer et al., 2007; Aslan et al., 2011; Gucer and Aslan, 2014). Following this metamorphic event, these rocks were obducted onto the Eastern Pontides in a sub-ophiolitic position. In agreement with Okay and Şahintürk (1997), we propose that the low-grade metamorphism documented for the YMR occured during shallow burial to greenschist facies conditions in an accretionary prism during intra-oceanic Neotethyan subduction. The YMR unit might thus represent a volcanic arc dragged below the ophiolite nappe when the SAB-TAP entered the subduction zone.

The question of the relationship of the YMR with the other sub-ophiolite metamorphic units in Armenia (Stepanavan and Amasia) is thus promted: do the the Armenian sub-ophiolitic units represent higher grade equivalents of the YMR or do they reflect distinct tectonic units with their own geodynamic significance?

The Amasia garnet-amphibolite and Stepanavan blueschist units bear higher metamorphic grades and distinct protoliths respect to the YMR. As these two units include some lithologies originating from the ocean floor, they may rather represent a marginal basin (Amasia) or an accretionary prism (Stepanavan), considering their respective metamorphic imprints. Indeed, these two units are clearly distinct from each other despite their geographic proximity (50 km; Fig. 2) and their high metamorphic grade. The P-T estimates for eclogite and amphibolite lithologies are too different from one another, being representative of distinct geothermal gradients to propose that they might represent a similar geodynamic context during their metamorphism. The 5 Myr age difference between them further argues that their formation is related to different geodynamic events: a subduction event at 95 Ma in Stepanavan and an obduction event in Amasia at 90 Ma. The metamorphic units of Stepanavan and Amasia are thus distinctively different units.

Being different units indicative of ascribed to distinct geodynamic events does not mean that they are not linked. The intra-oceanic subduction (i.e. Stepanavan sub-ophiolitic metamorphic unit, YMR) occurring prior to obduction (i.e. Amasia metamorphic sole) is thought to have facilitated the initiation of obduction of the Northern Neotethys onto the SAB, dated some 5 Myr later. Therefore, it is suggested that the arrival of the SAB in the subduction zone at c. 94-95 Ma may have blocked it and triggered overthrusting of the hot oceanic lithosphere (Hässig et al., 2016b; 2017).

Model for the Lesser Caucasus obduction

From all the available geological data, particularly with new P-T-t data from the amphibolites of the Amasia ophiolite metamorphic sole, we propose the following model for the evolution of the northern branch of Neotethys (Fig. 15):

1 - The magmatic rocks of the Amasia ophiolites, along with correlated ophiolites from the Lesser Caucasus and Northeastern Anatolia region, share similar geochemical signatures influenced by a subduction component in an oceanic basin environment (Hässig et al., 2013b). These data argue for simultaneous crust formation in a supra-subduction setting in the Middle to Late Jurassic times.

2 - Two north-dipping subduction zones are evidenced by simultaneous magmatism on the Eurasian active margin and in an intra-oceanic setting, responsible for the formation of the Supra Subduction Zone (SSZ) type ophiolite nappes (Fig. 15A, e.g., Galoyan et al., 2009; Rolland et al., 2009b; 2010). The intra-oceanic subduction is argued to continue until arrival of the SAB. Thus, the obduction contact accountable for ophiolite emplacement is thought to initiate at the back of the intra-oceanic subduction zone (Fig. 15C-D-E), which corresponds to the tectonic boundary limiting the southern edge of the Northern Branch of the Neotethys.

3 - Two magmatic suites were emplaced on top of each other: (1) a gabbroic basement of thinned back-arc oceanic crust, (2) topped by thick basaltic flows with an alkaline tendency. The presence of identical alkaline basalts in similar stratigraphic positions strongly favours the formation of several oceanic islands or one large plateau related to hot spot magmatism (Rolland et al., 2009b; Okay et al., 2013). Observations undertaken in the Amasia area are thus compatible with a model of obduction of a Supra Subduction Zone ophiolitic domain through intra-oceanic subduction and active oceanic margin slicing after OIB emplacement, which was successfully tested by numerical modelling (Fig. 15B; Hässig et al., 2016a; 2016b). This model explains the position of alkaline rocks both underneath, as sheared lenses occur in the mélange, and also above ophiolite as pillow lavas. These alkaline basalts would have been under-thrusted during intra-oceanic subduction or during emplacement of the overriding ophiolite nappes.

4 - The timing of pre- and post-obduction sediment sequences constrain the obduction to Coniacian-Santonian times, i.e. ≤ 89.8 Ma and ≥ 89.8 Ma (Sosson et al., 2010; Hässig et al., 2013a; Danelian et al., 2014). This is a rare example on Earth where metamorphic rocks yield similar ages as syn-tectonic sediments, which agrees for a fast obduction process dragging the deep metamorphic sole on top of superficial rocks within 5 Myr (Figs. 15Eand 15F).

5 - The hypothesis of ophiolite formation during intra-oceanic subduction raises the question of the location of the corresponding volcanic arc in Armenia. There, the only evidence of such an island arc can be found in the sub-ophiolitic

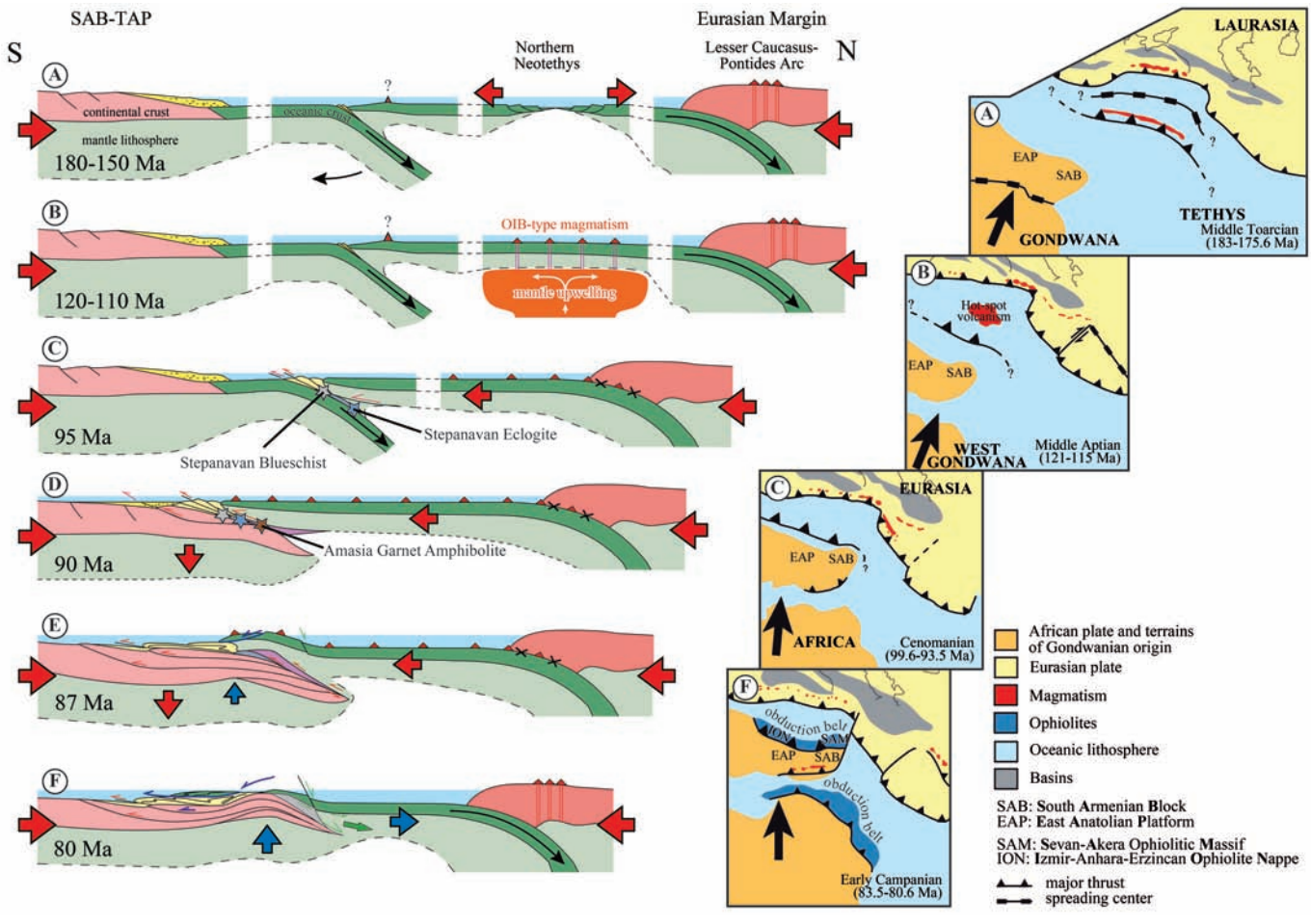

Fig. 15 - Middle Toarcian (c. 180 Ma) to Early Campanian (c. 83 Ma) palaeotectonic evolution of the Lesser Caucasus region and its neighbouring areas. The sketch cross-sections, modified after Hässig et al. (2016a), feature the results from this study. The maps are modified from Middle East Basins Evolution Programme palaeotectonic maps of the Middle East (Barrier and Vrielynck, 2008) to include our new data.

metamorphic units through the geochemical composition of metamorphic rocks. Two hypotheses on the disappearance of this arc may be proposed: (1) the alteration and erosion of the volcanic arc by uplift during the obduction or (2) the accretion and subduction of the fore-arc block and dragging of the volcanic arc with it, as proposed by Shemenda (1994) in his analogical model of subduction. This latter model is preferred based on:

(1) The presence of some compositions reflecting arc-related formation in the Stepanavan blueschists in Armenia. There, it is proposed that the Stepanavan blueschists correspond to the missing volcanic arc dragged into the subduction zone (Galoyan et al., 2007; Rolland et al., 2009a) (Fig. 15B-C). Further, some un-metamorphosed calc-alkaline lavas are found on top of the obducted section in Stepanavan (Galoyan et al., 2007), which is in agreement with a short volcanic arc episode during the obduction. Subduction of the arc could explain the relatively hot geothermal gradients obtained from both Stepanavan blueschists and Amasia amphibolites (e.g., Harper et al., 1996).

(2) More to the west, in northeastern Turkey, to the north of Erzincan, the YMR likely represents a metamorphosed equivalent of a SSZ intra-oceanic volcanic arc, (see section 7.3). Therefore, the absence of the volcanic arc formed above the intra-oceanic subduction may be explained by its accretion to the subducting slab and its dragging under the obducting ophiolite through scaling by faulting and tectonic erosion into the subduction channel. The latter gradually evolved into an "obduction channel" due to variations in the sinking slab dip.

Comparisons with other obductions in the Caucasus-Arabic domain

When considering the timing of obductions in the Middle East region it appears that the Lesser Caucasus and Oman ophiolites were obducted within the same time span (~90 Ma) (e.g., Agard et al., 2007; 2014 and references therein). However, preliminary paleomagnetic analyses show that both ophiolites were in distinct geographical locations distant of about 1200 km (Meijers et al., 2015). Further, these authors propose that a > 100 km large ocean domain still separated the SAB-TAP from the Southern Eurasian margin until Late Cretaceous times. Thus, synchronous southward obductions initiated within northern and southern Neotethyan oceanic basins, before a final subduction stage and final continental collision, at least for the Northern Neotethyan ophiolites. Linking the history of metamorphic rocks to that of syn- to post-obduction sediments from the southerly Vedi area and paleomagnetic data, gives strong arguments to infer that at the end of the obduction event (Coniacian-Santonian, 89.6 ± 0.5 to 83.6±0.2 Ma) a residual oceanic domain (less than 1000 km) still remained to be closed north of the obduction zone before final SAB-TAP collision with the Eurasian margin (Meijers et al., 2015).

Comparisons with central-western Turkey

There are similarities between the sub-ophiolite metamorphic complexes of Amasia, Stepanavan and Erzincan with those found at a larger scale in central and western Turkey. There, subduction/obduction initiation has been proposed at 92-95 Ma (e.g., Sherlock et al., 1999; Çelik et al., 2006, Plunder et al., 2015). The sub-ophiolitic metamorphic rocks are ultra-high pressure continental unit (P = 24 kbar, T = 500°C), eclogite (P = 17 kbar, T = 450°C) and blueschist (P = 11 kbar, T = 350°C) dated at 80 Ma, as well as metamorphic sole amphibolite (P = 11 kbar, T = 750°C), low grade metamorphosed oceanic lithosphere (4 ≤ P ≤ 8 kbar, T = 250 to 300°C) dated at 92 Ma (Sherlock et al., 1999, Plunder et al., 2015). Contrary to western Turkey, in the Erzincan, Amasia and Stepanavan regions, the MP/LP-HT metamorphism postdates the HP-MT/LT metamorphism. Differences also include the values of pressure and temperature in each of the two areas for the metamorphic rocks ascribed to each facies and geodynamic event. In western Turkey, the conditions recorded by the metamorphic sole amphibolite units are of higher pressure and temperature than for Amasia (P = 6.5 kbar, T = 600°C) . The metamorphic conditions of the sub-ophiolitic, subduction related, blueschists (P = 12 kbar, T = 550°C) and eclogites (P = 18.5 kbar, T = 590°C) of Stepanavan represent similar pressures but are hotter conditions than those in western Turkey. However, these differences might represent different 'snapshots' within a globally similar geodynamic context, involving a unique ophiolite nappe emplaced above the whole Anatolian micro-continent.

CONCLUSION

The petrologic study of Amasia and Stepanavan ophiolite argues for the presence of metamorphic rocks preserved in an ophiolite 'sole', below an un-metamorphosed ophiolite nappe. The metamorphic rocks preserve two successive parageneses featured by (1) S_1 deformation and amphibole-garnet-plagioclase crystallization at the HT peak and (2) a S_2 retrograde deformation and crystallization of phengite-chlorite-epidote. Thermobarometry indicates two distinct stages of a P-T path: an amphibolite stage at 6 ≤ P ≤ 7 kbar and T = 600±20°C kbar followed by a greenschist stage at 1.25 ≤ P ≤ 4.5 kbar and T = 350±30°C.

In this paper, this metamorphic sole is dated for the first time by direct in situ U-Pb dating of rutile (90.2±5.2 Ma) and $^{40}Ar/^{39}Ar$ dating on hornblende (87.7±5.6 Ma and 91.2±3.2 Ma) and white mica (phengite, 89.7±1.4 Ma) yielding for both S_1 and S_2 deformation stages similar within error ages of c. 90 Ma. In contrast, the study of the sub-ophiolitic metamorphic unit of the Stepanavan ophiolite has identified an eclogite stage at 17.5 < P < 20 kbar and T = 575±25°C, in addition to the previously constrained blueschist and greenschist stages. The new and previous datings account for a very rapid tectonic evolution featuring (1) the subduction oceanic lithosphere below a relatively hot oceanic lithosphere with slicing of the overriding oceanic domain at c. 95 Ma and (2) the underplating of this subducted material along the hanging wall of the intra-oceanic subduction at 90-87 Ma. The formation of the metamorphic sole marks a change in the geometry of the plate interface, with a shallowing of the subduction channel due to its flatting and rearrangement to become the obduction channel. Afterwards, (3) the garnet amphibolite unit was incorporated in a greenschist facies tectonic mélange at the base of the obducted ophiolite nappe (with blueschists and eclogite of Stepanavan formed during subduction) within the subsequent channel exhumation between 87 and 80 Ma. The end of obduction occurred thus after 1 to 7 Myr of its initiation, as shown by similar within-error of HT and LT metamorphic rocks with palaeontological ages in underlying and overlying Armenian foreland sediments, respectively.

ACKNOWLEDGMENTS

This work was supported by the MEBE and DARIUS programs coordinated by E. Barrier and M.F. Brunet from the University Pierre and Marie Curie and the INSU/CNRS. Fieldwork was facilitated by the support of the Armenian National Academy of Science (Institute of Geological Sciences). We wish to thank J.L. Devidal in Clermont-Ferrand, Delphine Bosch, Olivier Tottereau and Bernard Boyer in Montpellier, P. Capiez in Lyon and S. Gallet in Nice for their involvement during data acquisition. We also thank Chiara Frassi and an anonymous review for their constructive remarks. This publication is a contribution of "GEOAZUR", University of Nice-Sophia Antipolis, and CNRS, France.

REFERENCES

Abd El-Naby H., Frisch W. and Hegner E., 2000. Evolution of the Pan-African Wadi Haimur metamorphic sole, Eastern Desert, Egypt. J. Metam. Geol., 18: 639-651.

Adamia Sh. A., Chkhotua T., Kekelia M., Lordkipanidze M., Shavishvili I. and Zakariadze G., 1981. Tectonics of Caucasus and adjoining regions: implications for the evolution of the Tethys ocean. J. Struct- Geol. 3; 437-447.

Agard P., Jolivet L., Vrielynck B., Burov E. and Monié P., 2007. Plate acceleration: The obduction trigger? Earth Planet.Sci. Lette., 258: 428-441.

Agard P., Omrani J., Jolivet L., Whitechurch H., Vrielynck B., Spakman W. et al., 2011. Zagros orogeny: a subduction-dominated process. Geol. Mag., 148 (5-6): 692-725.

Agard P., Searle M.P., Alsop G.I. and Dubacq B., 2010. Crustal stacking and expulsion tectonics during continental subduction: P-T deformation constraints from Oman. Tectonics, 29: 1-19.

Agard P., Yamato P., Soret M., Prigent C., Guillot S., Plunder A., Dubacq B., Chauvet A. and Monié P., 2016. Plate interface rheological switches during subduction infancy: Control on slab penetration and metamorphic sole formation. Earth Planet. Sci. Lett., 451, 208-220.

Agard P., Zuo X., Funiciello F., Bellahsen N., Faccenna C. and Savva D., 2014. Obduction: Why, how and where, Clues from analog models. Earth Planet. Sci. Lett., 393: 132-145.

Al-Riyami K., Robertson A., Dixon J. and Xenophontos C., 2002. Origin and emplacement of the Late Cretaceous Baer-Bassit ophiolite and its metamorphic sole in NW Syria. Lithos, 65: 225-260.

Angiboust S., Pettke T., De Hoog J. C., Caron B. and Oncken O., 2014. Channelized fluid flow and eclogite-facies metasomatism along the subduction shear zone. J. Petrol., 55 (5): 883-916.

Asatryan G., Danelian T., Sosson M., Sahakyan L., Person A., Avagyan A. and Galoyan G., 2010. Radiolarian ages of the sedimentary cover of Sevan ophiolite (Armenia, Lesser Caucasus). Ofioliti, 35, 91-101.

Aslan Z., Gücer M.A. and Arslan M., 2011. ^{39}Ar-^{40}Ar dating on plagioclases of metabasic metagranitic rocks in the Yoncayolu metamorphic, NE Turkey. Miner. Mag., 75: 398-464.

Barrier E. and Vrielynck B., 2008. Palaeotectonic map of the Middle East, Atlas of 14 maps, Tectonosedimentary-Palinspastic maps from Late Norian to Pliocene. Commission for the Geologic Map of the World (CCMW, CCGM), Paris, France.

Barrier E., Vrielynck B., Brouillet J.F. and Brunet M.F. (Contributors: Angiolini L., Kaveh F., Poisson A., Pourteau A., Plunder A., Robertson A., Shekawat R., Sosson M., Zanchi A.), 2018. Paleotectonic reconstruction of the Central Tethyan Realm. Tectonono-sedimentary-palinspastic maps from Late Permian to Pliocene. CCGM/CGMW, Paris, http://www.ccgm.org. Atlas of 20 maps (scale: 1/15 000 000).

Beccaletto L. and Jenny C., 2004. Geology and correlation of the Ezine zone: A Rhodope fragment in NW Turkey? Turk. J. Earth Sci., 13: 145-176.

Bortolotti V., Marroni M., Pandolfi L. and Principi G., 2005. Mesozoic to Tertiary tectonic history of the Mirdita ophiolites, northern Albania. Island Arc, 14: 471-493.

Bortolotti V. and Sagri M., 1968. Ricerche sulle ofioliti delle catene alpine. 4-Osservazioni sull'età e la giacitura delle ofioliti tra Smirne ed Erzurum (Turchia). Boll. Soc. Geol. It., 87: 661-666.

Bruguier O., Bosch D., Caby R., Vitale-Brovarone A., Fernandez L., Hammor D., Laouar R., Ouabadi A., Abdallah N. and Mechati M., 2017. Age of UHP metamorphism in the Western Mediterranean: Insight from rutile and minute zircon inclusions in a diamond-bearing garnet megacryst (Edough Massif, NE Algeria). Earth Planet. Sci. Lett., 474: 215-225.

Carosi R., Cortesogno L., Gaggero L. and Marroni M., 1996. Geological and petrological features of the metamorphic sole from the Mirdita nappe, northern Albania. Ofioliti: 21, 21-40.

Çelik Ö.F., Delaloye M.F., Feraud G., 2006. Precise $^{40}Ar/^{39}Ar$ ages from the metamorphic sole rocks of the Tauride Belt Ophiolites, southern Turkey: implications for the rapid cooling history. Geol. Mag.,143: 213-227.

Cherniak D.J., 2000. Pb diffusion in rutile. Contrib. Miner. Petrol., 139: 198-207.

Coleman R.G., 1971. Plate tectonic emplacement of upper mantle peridotites along Continental edges. J. Geophys. Res., 76: 1212-1222.

Coleman R.G., 1981. Tectonic setting for ophiolite obduction in Oman. J. Geophys. Res., 86: 2497-2508.

Danelian T., Asatryan G., Galoyan G., Sahakyan L. and Stepanyan J., 2016. Late Jurassic-Early Cretaceous radiolarian age constraints from the sedimentary cover of the Amasia ophiolite (NW Armenia), at the junction between the Izmir-Ankara-Erzinçan and Sevan-Hakari suture zones. Intern. J. Earth Sci. (Geol. Rund.), 105: 67-80.

Danelian T., Asatryan G., Galoyan G., Sosson, M., Sahakyan L., Caridroit M. and Avagyan A., 2012. Geological history of ophiolites in the Lesser Caucasus and correlation with the Izmir-Ankara-Erzincan suture zone: insights from radiolarian biochronology. Bull. Soc. Géol. Fr., 183: 331-342.

Danelian T., Asatryan G., Sahakyan L., Galoyan G., Sosson M. and Avagyan A., 2010. New and revised radiolarian biochronology for the sedimentary cover of ophiolites in the Lesser Caucasus (Armenia). In: M. Sosson, N. Kaymakci, R.A. Stephenson, F. Bergerat and V. Starostenko (Eds.), Sedimentary basin tectonics from the Black Sea and Caucasus to the Arabian Platform. Geol. Soc. London Spec. Publ., 340: 383-391.

Danelian T., Asatryan G., Sosson M., Person A., Sahakyan L. and Galoyan G., 2008. Discovery of Middle Jurassic (Bajocian) Radiolaria from the sedimentary cover of the Vedi ophiolite (Lesser Caucasus, Armenia). C.R. Pal. Evol., 7: 327-334.

Danelian T., Galoyan G., Rolland Y. and Sosson M. 2007. Palaeontological (radiolarian) Late Jurassic age constraint for the Stepanavan ophiolite (Lesser Caucasus, Armenia). Bull. Geol. Soc. Greece, 40: 31-38.

Danelian T., Zambetakis-Lekkas A., Galoyan G., Sosson M., Asatryan G., Hubert B. and Grigiryan A., 2014. Reconstructing Upper Cretaceous (Cenomanian) paleoenvironments in Armenia based on radiolarian and benthic foraminifera; implications for the geodynamic evolution of the Tethyan realm in the Lesser Caucasus. Palaeo. Palaeo. Palaeo., 413: 123-132.

Dercourt J., Zonenshain L.P., Ricou L.-E., Kazmin V.G., Le Pichon X., Knipper A.L., et al., 1986. Geological evolution of the Tethys belt from the Atlantic to the Pamirs since the Lias. Tectonophysic, 123: 241-315.

Dewey J.F., 1976. Ophiolite obduction. Tectonophysics, 31: 93-120.

Dilek Y. and Whitney D., 1997. Counterclockwise P-T-t trajectory from the metamorphic sole of a Neo-Tethyan ophiolite (Turkey). Tectonophysics, 280: 295-310.

Ding L., Kapp P. and Wan X., 2005. Paleocene-Eocene record of ophiolite obduction and initial India-Asia collision, south central Tibet. Tectonics, 24: 1-9.

Duretz T., Agard P., Yamato P., Ducassou C., Burov E. and Gerya T., 2015. Thermo-mechanical modeling of the obduction process based on the Oman Ophiolite case. Gondw. Res., http://dx.doi.org/10.1016/j.gr.2015.02.002.

Elitok Ö. and Drüppel K. 2008. Geochemistry and tectonic significance of metamorphic sole rocks beneath the Beyşehir-Hoyran ophiolite (SW-Turkey). Lithos., 100: 322-353.

Engi M., Berger A. and Roselle G.T., 2001. Role of the tectonic accretion channel in collisional orogeny. Geology, 29: 1143-1146.

Gaggero L., Marroni M., Pandolfi L., Buzzi L., 2009. Modeling the oceanic lithosphere obduction: Constraints from the metamorphic sole of Mirdita ophiolites (Northern Albania). Ofioliti, 34: 17-42.

Galoyan G., Rolland Y., Sosson M., Corsini M., Billo S., Verati C. and Melkonyan R., 2009. Geology, geochemistry and $^{40}Ar/^{39}Ar$ dating of Sevan ophiolites (Lesser Caucasus, Armenia): Evidence for Jurassic Back-arc opening and hot spot event between the South Armenian Block and Eurasia. J. Asian Earth Sci., 34: 135-153.

Galoyan G., Rolland Y., Sosson M., Corsini M. and Melkonyan R., 2007. Evidence for superposed MORB, oceanic plateau and volcanic arc series in the Lesser Caucasus (Stepanavan, Armenia). C.R. Geosci., 339: 482-492.

Gao X.Y., Zheng Y.F., Xia X.P. and Chen Y.X., 2014. U-Pb ages and trace elements of metamorphic rutile from ultrahigh-pressure quartzite in the Sulu orogen. Geochim. Cosmochim. Acta, 143: 87-114.

Gasser D., Jeřábek P., Faber C., Stünitz H., Menegon L., Corfu F., Erambert M. and Whitehouse M.J., 2015. Behaviour of geochronometers and timing of metamorphic reactions during deformation at lower crustal conditions: phase equilibrium modelling and U-Pb dating of zircon, monazite, rutile and titanite from the Kalak Nappe Complex, northern Norway. J. Metam. Geol., 33: 513-534.

Gerya T.V., Stöckhert B. and Perchuk A.L., 2002. Exhumation of high-pressure metamorphic rocks in a subduction channel: A numerical simulation. Tectonics, 21: 6-1-6-15.

Gnos E., 1992. The metamorphic rocks associated with the Semail Ophiolite (Sultanate of Oman and United Arab Emirates). PhD Thesis, Univ. Berne, Switzerland, 120 pp.

Göncüoğlu M.C. and Turhan N., 1984. Geology of the Bitlis metamorphic belt. In: O. Tekeli and M.C. Göncüoğlu (Eds.), Geology of the Taurus Belt. Proceed. Intern. Symp., MTA, Ankara, p. 237-244,

Gray D.R. and Gregory R.T., 2000. Implications of the structure of the Wadi Tayin metamorphic sole, the Ibra-Dasir block of the Samail ophiolite, and the Saih Hatat window for late stage extensional ophiolite emplacement, Oman. Mar. Geophys. Res., 21: 211-227.

Gücer M.A., Aslan Z. and Bektas O., 2007. Petrology and geochemistry features of the Yoncayolu Metamorphics in Erzincan, NE Turkey. Geochim. Cosmochim. Acta, 71: A302-A366.

Guilmette C., Hébert R., Wang C. and Villeneuve M., 2009. Geochemistry and geochronology of the metamorphic sole underlying the Xigaze Ophiolite, Yarlung Zangbo Suture Zone, South Tibet. Lithos, 112: 149-162.

Hacker B.R., 1991. The role of deformation in the formation of metamorphic field gradients: Ridge subduction beneath the Oman ophiolite. Tectonics, 10: 455-473.

Hacker B.R. and Gnos E., 1997. The corundrum of Samail: explaining metamorphic history. Tectonophysics, 279: 215-226.

Hacker B.R., Mosenfelder J.L. and Gnos E., 1996. Rapid emplacement of the Oman ophiolite: Thermal and geochronologic constraints. Tectonics, 15: 1230-1247.

Harper G.D., Grady K. and Coulton A.J., 1996. Origin of the amphibolite "sole" of the Josephine ophiolite: Emplacement of a cold ophiolite over a hot arc. Tectonics, 15: 296-313.

Hässig M., Rolland Y., Duretz T. and Sosson M., 2016a. Obduction triggered by regional heating during plate reorganization. Terra Nova, 28: 76-82.

Hässig M., Duretz T., Rolland Y. and Sosson M., 2016b. Obduction of old oceanic lithosphere due to reheating and plate reorganization: insights from numerical modelling and the NE Anatolia-Lesser Caucasus case example. J. Geodyn., 96: 35-49.

Hässig M., Rolland Y., Sahakyan L., Sosson M., Galoyan Avagyan A. and Müller C., 2015a. Multi-stage metamorphism in the South Armenian Block during the Late Jurassic to Early Cretaceous: tectonics over south-dipping subduction of Northern branch of Neotethys. J. Asian Earth Sci., 102: 4-23.

Hässig M., Rolland Y. and Sosson M. 2017. From ocean crust genesis to obduction initiation: history of the northern branch of Neotethys prior to the Late Cretaceous obduction event in the NE Anatolian and Lesser Caucasus regions. In: M. Sosson, R.A. Stephenson and S.A. Adamia (Eds.), Tectonic evolution of the eastern Black Sea and Caucasus. Geol. Soc. London Spec. Publ., 428: 41-60.

Hässig M., Rolland Y., Sosson M. and Avagyan A., 2016c. Lithological nature of the subduction channel: Insights from the Karabakh suture zone (Lesser Caucasus) and general comparisons. J. Geodyn., 96: 19-34.

Hässig M., Rolland Y., Sosson M., Galoyan G., Müller C., Avagyan A. and Sahakyan L., 2013a. New structural and petrological data on the Amasia ophiolites (NW Sevan-Akera suture zone, Lesser Caucasus): Insights for a large-scale obduction in Armenia and NE Turkey. Tectonophysics, 588: 135-153.

Hässig M., Rolland Y., Sosson M., Galoyan G., Sahakyan L., Topuz G., Çelik Ö.F., Avagyan A. and Müller C., 2013b. Linking the NE Anatolian and Lesser Caucasus ophiolites: evidence for large scale obduction of oceanic crust and implications for the formation of the Lesser Caucasus-Pontides Arc. Geodyn. Acta, 26: 311-330.

Hempton M.R., 1985. Structure and deformation history of the Bitlis Suture near Lake Hazar, SE Turkey. Geol. Soc. Am. Bull., 96: 223-243.

Holland T.J.B. and Powell R., 2003. Activity-composition relations for phases in petrological calculations: an asymmetric multicomponent formulation. Contrib. Miner. Petrol., 145: 492-501.

Knipper A.L., 1975. The oceanic crust in the structure of the Alpine Folded Belt (South Europe, western part of Asia and Cuba). Transact. 267, Moscow 'Nauka', 207 (in Russian).

Knipper A.L. and Khain E.V., 1980. Structural position of ophiolites of the Caucasus. In: G. Rocci (Ed.), Tethyan ophiolites, Ofioliti, Spec. Iss., 2: 297-314.

Knipper A.L., Ricou L.E and, Dercourt J., 1986. Ophiolites as indicators of the geodynamic evolution of the Tethyan ocean. Tectonophysics, 123: 213-240.

Kooijman E., Mezger K. and Berndt J., 2010. Constraints on the U-Pb systematics of metamorphic rutile from in situ LA-ICP-MS analysis. Earth Planet. Sci. Lett., 293 (3-4): 321-330.

Kooijman E., Smit M.A., Mezger K. and Berndt J., 2012. Trace element systematics in granulite facies rutile: implications for Zr geothermometry and provenance studies. J. Metam. Geol., 30: 397-412.

Leake B.E., Woolley A.R., Arps C.E.S., Birch W.D., Gilbert M.C., Grice J.D., Hawthrne FC., et al., 1997. Nomenclature of amphiboles: report of the subcommittee on amphiboles of the International Mineralogical Association, Commission on new minerals and mineral names. Can. Miner., 35: 219-246.

Lytwyn J.N., Casey J.F., 1995. The geochemistry of postkinematic mafic dike swarms and sub-ophiolitic metabasites, Pozantı-Karsantı ophiolite, Turkey: evidence for ridge subduction. Geol. Soc. Am. Bull., 10: 830-850.

Massonne H.-J. and Schreyer W., 1987. Phengite geobarometry based on the limiting assemblage with K-feldspar, phlogopite, and quartz. Contrib. Miner. Petrol., 96: 212-224.

McDougall I. and Harrison T.M., 1999. Geochronology and thermochronology by the $^{40}Ar/^{39}Ar$ Method. Oxford University Press, 296 pp.

Mederer J., Moritz R., Ulianov A. and Chiaradia M., 2013. Middle Jurassic to Cenozoic evolution of arc magmatism during Neotethys subduction and arc-continent collision in the Kapan Zone, southern Armenia. Lithos, 177: 61-78.

Meijers M., Smith B., Kircher U., Mensink M., Sosson M., Rolland Y., Grigoryan A., Sahakyan L., Avagyan A., Langereis C. and Müller C., 2015. A paleolatitude reconstruction of the South Armenian Block (SAB) since the Late Cretaceous: constraints on the Tethyan realm. Tectonophysics, 644-645: 197-219, doi: 10.1016/j.tecto.2015.01.012.

Meijers M.J., Smith B., Pastor-Galán D., Degenaar R., Sadradze N., Adamia S., Sahakyan L., Avagyan A., Sosson M., Rolland Y., Langereis C.G. and Müller C., 2017. Progressive orocline formation in the Eastern Pontides-Lesser Caucasus. In: M. Sosson, R.A. Stephenson and S.A. Adamia (Eds.), Tectonic evolution of the eastern Black Sea and Caucasus. Geol. Soc. London Spec. Publ., 428: 117-143.

Michard A., Boudier F. and Goffé B., 1991. Obduction versus subduction and collision in the Oman case and other Tethyan settings. Petrol. Struc. Geol., 5: 447-467.

Moritz R., Rezeau H., Ovtcharova M., Tayan R., Melkonyan R., Hovakimyan S., Ramazanov V., Selby D., Ulianov A., Chiaradia M. and Putlitz B., 2016. Long-lived, stationary magmatism and pulsed porphyry systems during Tethyan subduction to post-collision evolution in the southernmost Lesser Caucasus, Armenia and Nakhitchevan. Gondw. Res., 37: 465-503.

Oberhänsli R., Candan O., Bousquet R., Rimmele G., Oka, A. and Goff J., 2010. Alpine HP evolution of the eastern Bitlis complex, SE Turkey. In: M. Sosson, N. Kaymakci, R. Stephanson, F. Bergarat and V. Storatchenoko (Eds.), Sedimentary basin tectonics from the Black Sea and Caucasus to the Arabian Platform. Geol. Soc. London Spec. Publ., 340: 461-483.

Oberhänsli R., Koralay E., Candan O., Pourteau A. and Bousquet R., 2014. Late Cretaceous ecologitic high-pressure relics in the Bitlis Massif. Geodin. Acta, 26: 175-190.

Okay A.I. and Topuz G., 2017. Variscan orogeny in the Black Sea region. Intern. J. Earth Sci., 106 (2): 569-592.

Okay A.I. and Tüysüz O., 1999. Tethyan sutures of northern Turkey. In: B. Durand, L. Jolivet, F. Horváth and M. Séranne, (Eds.), The Mediterranean Basins: Tertiary extension within the Alpine orogeny. Geol. Soc. London Spec. Publ., 156: 475-515.

Okay A.I., Sunal G., Sherlock S., Altıner D., Tüysüz O., Kylander-Clark A.R.C. and Aygül M., 2013. Early Cretaceous sedimentation and orogeny on the active margin of Eurasia: Southern Central Pontides, Turkey. Tectonics, 32: 1247-1271.

Okay A.I., Tansel I. and Tüysüz O., 2001. Obduction, subduction and collision as reflected in the Upper Cretaceous-Lower Eocene sedimentary record of western Turkey. Geol. Mag., 138: 117-142.

Palandjyan S.A., 1971. The petrology of ultrabasic and gabbroic rocks of the Sevan mountain range. Izdatelstvo NAS Armenian SSR, 201 (in Russian).

Parlak O., Çolakoğlu A., Dönmez C., Sayak H., Yildirim N., Türkel A. and Odabaşi İ., 2013. Geochemistry and tectonic significance of ophiolites along the Ankara-Erzincan suture zone in northeastern Anatolia. In: A.H.F. Robertson, O. Parlak and U.C. Ünlügenç (Eds.), Geological Development of Anatolia and the Easternmost Mediterranean Region. Geol. Soc. London Spec. Publ., 372: 75-105.

Pearce J.A., 1982. Trace element characteristics of lava from destructive plate boundaries. In: R.S. Thorpe (Ed.), Andesites. Wiley, New York, p. 525-548.

Pearce J.A., 1996. A users guide to basalt discrimination diagrams. In: D.A. Wyman (Ed.), Trace element geochemistry of volcanic rocks: applications for massive sulphide exploration. Geochemistry short course notes. Geol. Ass. Can., 12: 79-113.

Pearce J.A., Lippard S.J. and Roberts S., 1984. Characteristics and tectonic significance of suprasubduction zone ophiolite. In: B.P. Kokelaar and M.F. Howells (Eds.), Marginal basin geology. Geol. Soc. London Spec. Publ., 16: 77-94.

Penniston-Dorland S.C., Kohn M.J. and Manning C.., 2015. The global range of subduction zone thermal structures from exhumed blueschists and eclogites: Rocks are hotter than models. Earth Planet. Sci. Lett., 428: 243-254.

Perfit M.R., Gust D.A., Bence A.E., Arculus R.J. and Taylor S.R., 1980. Chemical characteristics of island-arc basalts: implications for mantle sources. Chem. Geol., 30: 227-256.

Plunder A., Agard P., Chopin C., Pourteau A. and Okay A.I., 2015. Accretion, underplating and exhumation along a subduction interface: From subduction initiation to continental subduction (Tavşanlı zone, W. Turkey). Lithos, 226: 233-254.

Plunder A., Agard P., Chopin C., Soret M., Okay A.I. and Whitechurch H., 2016. Metamorphic sole formation, emplacement and blueschist facies overprint: Early subduction dynamics witnessed by western Turkey ophiolites. Terra Nova, 28: 329-339.

Pourteau A., Sudo M., Candan O., Lanari P., Vidal O. and Oberhänsli R., 2013. Neotethys closure history of Anatolia: insights from ^{40}Ar-^{39}Ar geochronology and P-T estimation in high-pressure metasedimentary rocks. J. Metam. Geol., 31: 585-606.

Rezeau H., Moritz R., Leuthold J., Hovakimyan S., Tayan R. and Chiaradia M., 2017. 30 Myr of Cenozoic magmatism along the Tethyan margin during Arabia-Eurasia accretionary orogenesis (Meghri-Ordubad pluton, southernmost Lesser Caucasus). Lithos, 288: 108-124.

Rezeau, H., Moritz R., Wotzlaw J.F., Tayan R., Melkonyan R., Ulianov A., Selby D., d'Abzac F.-X. and Stern R.A., 2016. Temporal and genetic link between incremental pluton assembly and pulsed porphyry Cu-Mo formation in accretionary orogens. Geology, 44: 627-630.

Rice S.P. Robertson A.H.F., Ustaömer T., Inan N. and Tasli K., 2009. Late Cretaceous-Early Eocene tectonic development of the Tethyan suture zone in the Erzincan area, Eastern Pontides, Turkey. Geol. Mag., 146: 567-590.

Ricou L.E., Zonenshain L.P., Dercourt J., Kazmin V.G., Le Pichon X., Knipper A.L., et al., 1985. Méthodes pour l'établissement de neuf cartes paléogéographiques de l'Atlantique au Pamir depuis le Lias. Bull. Soc. Géol. Fr. 8: 625-635.

Robertson A.H.F. and Karamata, S., 1994. The role of subduction-accretion processes in the tectonic evolution of the Mesozoic Tethys in Serbia. Tectonophysics, 234: 73-94.

Robertson A.H.F., Parlak O., Ustaömer T., Taslı K., İnan N., Dumitrica P. and Karaoğlan F., 2013. Subduction, ophiolite genesis and collision history of Tethys adjacent to the Eurasian continental margin: New evidence from the Eastern Pontides, Turkey. Geodin. Acta, 26: 230-293.

Rolland Y., Billo S., Corsini M., Sosson M. and Galoyan G., 2009a. Blueschists of the Amasia-Stepanavan Suture Zone (Armenia): linking Tethys subduction history from E-Turkey to W-Iran. Intern. J. Earth Sci., 98: 533-550.

Rolland Y., Galoyan G., Bosch D., Sosson M., Corsini M., Fornari M. and Vérati C., 2009b. Jurassic back-arc and hot-spot related series in the Armenian ophiolites - Implications for the obduction process. Lithos, 112: 163-187.

Rolland Y., Galoyan G., Sosson M., Melkonian R. and Avagyan A., 2010. The Armenian ophiolites: insights for Jurassic Back-arc formation, Lower Cretaceous hot-spot magmatism, and Upper Cretaceous obduction over the South Armenian Block. In: M. Sosson, N. Kaymakci, R. Stephanson, F. Bergarat and V. Storatchenoko (Eds.), Sedimentary basin tectonics from the Black Sea and Caucasus to the Arabian Platform. Geol. Soc. London Spec. Publ., 340: 353-382.

Rolland Y., Hässig M., Bosch D., Meijers M.J.M., Sosson M., Bruguier O., Adamia Sh. and Sadradze N., 2016. A review of the plate convergence history of the East Anatolia-Transcaucasus region during the Variscan: Insights from the Georgian basement and its connection to the Eastern Pontides. J. Geodyn., 96: 131-145.

Rolland Y., Perincek D., Kaymakci N., Sosson M., Barrier E. and Avagyan A., 2012. Evidence for ~ 80-75 Ma subduction jump during Anatolide-Tauride-Armenian block accretion and ~ 48 Ma Arabia-Eurasia collision in Lesser Caucasus-East Anatolia. J. Geodyn., 56: 76-85.

Rolland Y., Sosson M., Adamia Sh. and Sadradze N., 2011. Prolonged Variscan to Alpine history of an active Eurasian margin (Georgia, Armenia) revealed by $^{40}Ar/^{39}Ar$ dating. Gondw. Res., 20: 798-815.

Rollinson, H.R., 1993. Using geochemical data: evaluation, presentation, interpretation. Longman Scientific, Technical, New York, 352 pp.

Sahakyan L., Bosch D., Sosson M., Avagyan A., Galoyan G., Rollan, Y., Bruguier O., Stepanyand B. and Vardanyan S., 2017. Geochemistry of the Eocene magmatic rocks from the Lesser Caucasus area (Armenia): evidence of a subduction geodynamic environment. In: M. Sosson, R.A. Stephenson and S.A. Adamia (Eds.), Tectonic Evolution of the Eastern Black Sea and Caucasus. Geol. Soc. London Spec. Publ., 428: 73-98.

Searle, M., Cox, J., 1999. Tectonic setting, origin, and obduction of the Oman ophiolite. Geol. Soc. Am. Bull., 111: 104-122.

Sengör A.M.C. and Yilmaz Y., 1981. Tethyan evolution of Turkey: A plate tectonic approach. Tectonophysics, 75: 181-241.

Shemenda A.I., 1994. Subduction: Insights from physical modeling. Kluwer Acad. Publ., Dordrecht, 215 pp.

Sokolov S.D., 1977. The olistostromes and ophiolitic nappes of the Lesser Caucasus. Izdatelstvo 'Nauka', Moscow, 92pp. (in Russian).

Sosson M., Rolland Y., Danelian T., Muller C., Melkonya R., Adamia S., Kangarli A. and Galoyan G., 2010. Subductions, obduction and collision in the Lesser Caucasus (Armenia, Azerbaijan, Georgia), new insights. In: M. Sosson, N. Kaymakci, R.A. Stephenson, F. Bergerat and V. Starostenko (Eds.), Sedimentary Basin Tectonics from the Black Sea and Caucasus to the Arabian Platform. Geol. Soc. London Spec. Publ., 340: 329-352.

Sosson M., Stephenson R., Sheremet Y., Rolland Y., Adamia Sh., Melkonian R., Kangarli T., Yegorova T., Avagyan A., Galoyan G., Danelian T., Hässig M., Meijers M., Müller C., Sahakyan L., Sadradze N., Alania V., Enukidze O. and Mosar J., 2016. The eastern Black Sea-Caucasus region during the Cretaceous: New evidence to constrain its tectonic evolution. C.R. Geosci., 348: 23-32.

Spray J.G., 1983. Lithosphere- asthenosphere decoupling at spreading centers and initiation of obduction. Nature, 304: 253-255.

Stampfli G.M. and Borel G.D., 2002. A plate tectonic model for the Paleozoic and Mesozoic constrained by dynamic plate boundaries and restored synthetic oceanic isochrones. Earth Planet. Sci. Lett., 196: 17-33.

Stampfli G.M., Borel G.D., Cavazza W., Mosar J. and Ziegler P.A., 2001. Palaeotectonic and palaeogeographic evolution of the western Tethys and PeriTethyan domain (IGCP Project 369). Episodes, 24: 222-228.

Steiger R.H. and Jäger E., 1977. Subcommission on geochronology: convention on the use of decay constants in geo- and cosmochronology. Earth Planet. Sci. Lett., 36: 359-362.

Sun S.S. and McDonough W.F., 1989. Chemical and isotopic systematic of oceanic basalts: implications for mantle composition and processes. In: A.D. Saudners and M.J. Norry (Eds.), Magmatism in ocean basins. Geol. Soc. London Spec. Publ., 42: 313-345.

Syracuse E.M., van Keken P.E. and Abers G.A., 2010. The global range of subduction zone thermal models. Phys. Earth Planet. Inter., 183: 73-90.

Tartese R., Ruffet G., Poujol M., Boulvais P. and Ireland T.R., 2011. Simultaneous resetting of the muscovite K-Ar and monazite U-Pb geochronometers: a story of fluids. Terra Nova, 23 (6): 390-398.

Topuz G., Çelik Ö.F., Şengör C., Altıntaş E., Zack T., Rolland Y. and Barth M., 2013b. Jurassic ophiolite formation and emplacement as backstop to a subduction-accretion complex in NE Turkey and relation to the Balkan ophiolites. Am. J. Sci., 313: 1054-1087.

Topuz G., Göçmengil G., Rolland Y., Çelik Ö.F., Zack T. and Schmitt A.K., 2013a. Jurassic accretionary complex and ophiolite from northeast Turkey: No evidence for the Cimmerian continental ribbon. Geology, 41: 255-258.

Turner G., Huneke J.C., Podose F.A. and Wasserburg G.J., 1971. $^{40}Ar/^{39}Ar$ ages and cosmic ray exposure ages of Apollo 14 samples. Earth Planet. Sci. Lett., 12: 15-19.

Uunk B., Brouwer F., ter Voorde M. and Wijbrans J., 2018. Understanding phengite argon closure using single grain fusion age distributions in the Cycladic Blueschist Unit on Syros, Greece. Earth Planet. Sci. Lett., 484: 192-203.

Uysal I.E., Ersoy Y., Dilek Y., Escayola M., Sarıfakıoğlu E., Saka S. and Hirata T., 2015. Depletion and refertilization of the Tethyan oceanic upper mantle as revealed by the early Jurassic Refahiye ophiolite, NE Anatolia - Turkey. Gondw. Res., 27: 594-611.

Vaughan A.P. and Scarrow J.H., 2003. Ophiolite obduction pulses as a proxy indicator of superplume events? Earth Planet. Sci. Lett., 213: 407-416.

Villa I M., Hermann J., Müntener O. and Trommsdorff V., 2000. $^{39}Ar/^{40}Ar$ dating of multiply zoned amphibole generations (Malenco, Italian Alps). Contrib. Miner. Petrol., 140 (3): 363-381.

Vry J.K. and Baker J.A., 2006. LA-MC-ICPMS Pb-Pb dating of rutile from slowly cooled granulites: Confirmation of the high closure temperature for Pb diffusion in rutile. Geochim.t Cosmochim. Acta, 70: 1807-1820.

Warren C.J., Hanke F. and Kelley S.P., 2012. When can muscovite $^{40}Ar/^{39}Ar$ dating constrain the timing of metamorphic exhumation?. Chem. Geol., 291: 79-86.

Wakabayashi J. and Dilek Y., 2000. Spatial and temporal relationships between ophiolites and their metamorphic soles: A test of models of forearc ophiolite genesis. In: Y. Dilek, E.M. Moores, D. Elthon and A. Nicolas, (Eds.), Ophiolites and oceanic crust: New insight from field studies and the Ocean Drilling Program. Geol. Soc. Am. Spec. Pap., 349: 53-64.

Wakabayashi J. and Dilek Y., 2003. What constitutes 'emplacement' of an ophiolite?: Mechanisms and relationship to subduction initiation and formation of metamorphic soles. Geol. Soc. London Spec. Publ., 218: 427-447.

Whitechurch H., Juteau T. and Montigny R., 1984. Role of the Eastern Mediterranean ophiolites (Turkey, Syria, Cyprus) in the history of the Neo-Tethys. Geol. Soc. London Spec. Publ., 17: 301-317.

Whitney D.L. and Evans B.W., 2010. Abbreviations for names of rock-forming minerals. Am. Miner., 95: 185-187.

Yılmaz A., Adamia S. and Yılmaz H., 2014. Comparison of the suture zones along a geotravse from the Scythian Platform to the Arabian Platform. Geosci. Front., 5: 855-875.

Zakariadze G.S., Knipper A.L., Sobolev A.V., Tsamerian O.P., Dmitriev L.V., Vishnevskaya V.S. and Kolesov G.M., 1983. The ophiolite volcanic series of the Lesser Caucasus. Ofioliti, 8: 439-466.

Zakariadze G.S., Knipper A.L., Bibikova E.V., Silantiev S.A., Zlobin S.K., Gracheva T.V., Makarov S.A. and Kolesov T.M., 1990. The setting and age of the plutonic part of the NE Sevan ophiolite complex. Izvestia NAS USSR, 3: 17-30 (in Russian).

Received, March 16, 2018
Accepted, October 5, 2018

SUPPLEMENTARY DATA

Supplementary data
all supplementary data are available at the web page www.ofioliti.it

S1 - Analytical procedures.

S2 - Electron microprobe analyses of representative garnets from metamorphic rocks of the Amasia and Stepanavan ophiolite complexes. Oxydes and end-member proportions are given in percentages.

S3 - Electron microprobe analyses of representative amphiboles from metamorphic rocks of the Amasia ophiolite complex.

S4 - Electron microprobe analyses of representative chlorites from metamorphic rocks of the Amasia ophiolite complex.

S5 - Electron microprobe analyses of representative micas from metamorphic rocks of the Amasia ophiolite complex.

S6 - P-T pseudosection for sample AR-08-09c calculated with THERIAK-DOMINO.

S7 - P-T pseudosection for sample ARM-11-13 calculated with THERIAK-DOMINO.

S8 - (k390.full_1sigma), detailed $^{40}Ar/^{39}Ar$ results for amphibole from sample AR-09-08.

S9 - (k402.full_1sigma), detailed $^{40}Ar/^{39}Ar$ results for amphibole from sample AR-09-15.

S10 - (k427.full_1sigma), detailed $^{40}Ar/^{39}Ar$ results for amphibole from sample AR-08-09c.

S11 - (k428.full_1sigma), detailed $^{40}Ar/^{39}Ar$ results for white mica from sample AR-08-09c.

S12 - Laser ablation trace element analyses of rutile grains from samples AR09-08 and AR09-15.

Geochemical analysis

The sampling was undertaken throughout several field campaigns in 2008, 2009 and 2010. Samples from the Amasia ophiolite and related metamorphics were analyzed for major and trace elements, including Rare Earth Elements (REE; Table 1). Samples were analyzed at the C.R.P.G. (Nancy, France). Analytical procedures and analyses of standards can be found on the following website (http://www.crpg.cnrs-nancy.fr/SARM). Additional data pertaining to the other Armenian ophiolites are published in Galoyan et al. (2009) and Rolland et al. (2009b; 2010).

In order to designate geochemical affinities and corresponding tectonic environments for sampled rocks (Pearce and Cann, 1973; Floyd and Winchester, 1975; 1978; Pearce and Norry, 1979; Pearce, 1982; 1983; 1996) the option to study relatively immobile elements, such as Ti, Zr, Y, Nb, Ta, Th, V and REEs, was chosen because of their relative immobility throughout low grade submarine alteration (e.g, Hart et al., 1974; Humphris and Thompson, 1978) (Figs. 8A, B and C). Normal Mid Oceanic Ridge Basalt (N-MORB) normalized spidergrams for the Armenian ophiolites are presented in Fig. 8D. In Amasia, considering the geochemical data obtained from ophiolite samples and related metamorphic rocks, two tendencies are observed: suprasubduction tholeiitic and alkaline.

Petrography and mineral chemistry

Mineral compositions were determined by electron probe microanalysis (EPMA). The analyses are presented in Tables 2-5. They were carried out using a Cameca Camebax SX100 electron microprobe at 15 kV and 1 nA beam current, at the Blaise Pascal University (Clermont-Ferrand, France). Natural samples were used as standards.

$^{40}Ar/^{39}Ar$ Dating

Geochronology was undertaken by single-grain laser $^{40}Ar/^{39}Ar$ dating on different mineral phases, amphiboles and white micas for amphibolites and green-schists parageneses, respectively. $^{40}Ar/^{39}Ar$ dating results are presented in Table 6 and Fig. 11 and detailed in the Appendices S2-S5. The amphiboles and white mica were analyzed by EPMA prior to dating in order to check mineral composition homogeneity (Tables 2 and 4). Grains between 800 μm and 500 μm were separated by careful selection by hand-picking under a binocular microscope to prevent the presence of altered grains. The samples were then irradiated in the nuclear reactor at McMaster University in Hamilton (Canada), in position 5c, along with Hb3gr hornblende neutron flux monitor, for which an age of 1072 Ma is adopted (Turner et al., 1971). The total neutron flux density during irradiation was 9.0 x 10^{18} neutron cm^{-2}. The estimated error bar on the corresponding $^{40}Ar^*/^{39}Ar_K$ ratio is ± 0.2% (1r) in the volume where the samples were set. All $^{40}Ar/^{39}Ar$ measurements were undergone in the University of Nice-Sophia Antipolis (UMR 7329 Géoazur). Analyses of amphibole grains were undertaken by step heating with a 50 W CO_2 Synrad 48-5 continuous laser beam. Measurement of isotopic ratios was done with a VG3600 mass spectrometer equipped with a Daly detector system. Detailed procedures are described in Jourdan *et al.* (2004). The typical blank values for extraction and purification of the laser system are in the range 4.2 - 8.75, 1.2 - 3.9, and 2 - 6 cc STP for masses 40, 39 and 36, respectively. Mass discrimination was monitored by regularly analyzing air pipette volumes. Decay constants are those given by Steiger and Jäger (1977). Uncertainties on apparent ages are given at the 2σ level and do not include the error on the $^{40}Ar^*/^{39}Ar_K$ ratio of the monitor. Plateau and isochron age estimates are given with a 1σ error. Considering the homogeneous distribution of Ca/K values during the experiments and EPMA analysis, only one mineral phase has contributed to the $^{40}Ar/^{39}Ar$ signal in each sample.

U-Pb dating

LA-ICP-MS U-Th-Pb rutile analyses were performed in-situ on thin section. Analyses were carried out using a Lambda Physik CompEx 102 excimer laser generating 15 ns duration pulses of radiation at a wavelength of 193 nm. For analyses, the laser was coupled to an Element XR sector field ICP-MS (AETE-ISO regional facility of the OSU OREME, University of Montpellier). The instrument was tuned for maximum sensitivity and low oxide production (ThO/Th < 1%). Analytical conditions are identical to those reported in previous studies (e.g., Bosch et al., 2011; Bruguier et al., 2017) where ablation experiments were performed under helium, which enhances sensitivity and reduces inter-element fractionation (Gunther and Heinrich, 1999). The helium stream and particles ablated from the sample were mixed with Ar before entering the plasma. Laser spot size was 51 μm. The laser was operated at a repetition rate of 4Hz using a 12 J/cm^2 energy density. Total analysis time was 60s with the first 15s used for background measurement (laser disabled) which was substracted from the sample signal. Before each analysis, the surface of the targeted zone was cleaned with 10 pulses using a spot size twice larger than the size used for U-Pb analyses. All isotopes (202Hg, 204Pb + Hg, 206Pb, 207Pb, 208Pb, 238U and 232Th) were measured in pulse counting mode. The isotopes were measured using 15 points per peak and a 20% mass window resulting in 3 measured points for each mass station. Pb/U and Pb/Pb ratios were calibrated against the rutile reference material R10 (Luvizotto et al., 2009) which was measured four times each block of five unknowns. Reproducibility of the 207Pb/206Pb and 206Pb/238U ratios for the R10 standard was 0.4% and 1.1% respectively in the course of this study (n = 10). U-Pb isotopic data were reduced using GLITTER software (Reference) by carefully selecting the integration range for gas blank and sample. The decay constants and present-day 238U/235U value given by Steiger and Jäger (1977) were used and ages were calculated using the program Isoplot/Ex of Ludwig (2002).